# Exploring Metal Doped $B_{12}N_{12}$ Nanocage as Single Atom Catalyst for $CO_2$ Reduction to Formic Acid: A DFT-Driven Analysis

MS Thesis

by

Muqaddis Zahra

CIIT/SP24-R06-012/LHR

**COMSATS University Islamabad**

**Lahore Campus, Pakistan**

**Fall 2025**

# Exploring Metal Doped $B_{12}N_{12}$ Nanocage as Single Atom Catalyst for $CO_2$ Reduction to Formic Acid: A DFT-Driven Analysis

A Thesis Presented to

COMSATS University Islamabad, Lahore Campus

In partial fulfillment

of the requirement for the degree of

Master of Science

in

Chemistry

by

Muqaddis Zahra

CIIT/SP24-R06-012/LHR

Department of Chemistry

Faculty of Science

**Comsats University Islamabad**

**Lahore Campus, Pakistan**

**Fall 2025**

# Exploring Metal Doped $B_{12}N_{12}$ Nanocage as Single Atom Catalyst for $CO_2$ Reduction to Formic Acid: A DFT-Driven Analysis

This thesis submitted to the Department of Chemistry as partial fulfilment of the requirements for the award of Degree of MS in Chemistry.

| Name | Registration Number |
|---|---|
| Muqaddis Zahra | CIIT/SP24-R06-012/LHR |

## Supervisory Committee


**Supervisor**

Prof. Dr. Mazhar Amjad Gilani
Professor
Department of Chemistry
Comsats University Islamabad
CUI
Lahore Campus

**Co-Supervisor**

Dr. Sobia Tabassum
Associate Professor
IRCBM
Comsats University Islamabad CUI
Lahore Campus

**Member**

Dr. Sara Riaz

Associate Professor Department of Chemistry
Comsats University Islamabad (CUI)
Lahore Campus

# Final Approval

# Exploring Metal Doped $B_{12}N_{12}$ Nanocage as Single Atom Catalyst for $CO_2$ Reduction to Formic Acid: A DFT-Driven Analysis

By

*Muqaddis Zahra*

*CIIT/SP24-R06-012/LHR*

Has been approved

For the COMSATS University Islamabad, Lahore Campus

External Examiner: _____

Dr.

Supervisor: _____

Dr. Mazhar Amjad Gilani

Department of Chemistry, CUI, Lahore Campus

HoD: _____

Dr. Muhammad Shahid

Nazir

Department of Chemistry

CUI, Lahore Campus

# Author's Declaration

I, Muqaddis Zahra, CIIT/SP24-R06-012/LHR hereby declare that I have produced the work presented in this thesis, during the scheduled period of study. I also declare that I have not taken any material from any source except referred to wherever due to that amount of plagiarism is within acceptable range. ChatGPT was used for grammar correction. If a violation of HEC rules on research has occurred in this thesis, I shall be liable to punishable action under the plagiarism rules of the HEC.

Date: _____

Signature of the student:

Muqaddis Zahra

CIIT/SP24-R06-012/LHR

# Certificate

It is certified that Muqaddis Zahra, CIIT/SP24-R06-012/LHR has carried out all the work related to this thesis under my supervision at the Department of Chemistry, COMSATS University Islamabad, Lahore Campus and the work fulfill the requirements for award of MS degree.

Date: _____

Supervisor:

Dr. Mazhar Amjad Gilani

Professor

Department of Chemistry

COMSATS University Islamabad, Lahore Campus

## Dedication

This thesis is humbly dedicated to my parents whose unwavering prayers, love, and dedication have always been behind my every achievement. Your love is the driving force behind every word written and every milestone achieved.

# Acknowledgements

All praises are for **Allah** who is the **Creator** of the Universe. He is the most beneficent and most **merciful.** All gratitude and prayers belong to **Him** and peace be upon **Hazrat Muhammad (S.A.W)** His last messenger and servant. I am deeply grateful to **Allah Almighty** for giving me the strength to apprehend my work and for enabling me to stand strong and optimistic in ups and downs during the whole time.

First and foremost, I have a great inspiration for my supervisor, Dr. Mazhar Amjad Gilani (professor), CUI Lahore Campus, Pakistan, whose thoughtful suggestions and guidance as well as very compassionate and welcoming attitude kept me high-spirited throughout my research work. He has been supportive since the days I began working on the project in his lab

I would also like to express my gratitude to the head of the department Dr. Shahid Nazir and my teachers at CUI Lahore, including Dr. Sadaf ul Hassan, Dr. Sara Riaz and Dr. Lubna. Their pedagogy and keenness for their respective subjects made a strong impression on me and I have always carried great memories of their classes with me. I also express my appreciation for the rest of staff for their support and help towards my graduation.

Profound gratitude to my lab colleagues, **Ms. Tahreem Zahid** (MS scholar), **Mr. Syed Muhammad Zareef** (MS. scholar), **Ms**. **Amna Zafar** (MS scholar), **Arshia Irfan** (MS Scholar), **Ms. Fatima Mehmood** and other lab mates, for their continuous guidance and support.

Finally, yet importantly my heartfelt gratitude to my beloved parents and my siblings for their prayers, everlasting love and support.

Muqaddis Zahra

CIIT/SP24-R06-012/LHR

# Abstract

## Exploring Metal Doped $B_{12}N_{12}$ Nanocage as Single Atom Catalyst for $CO_2$ Reduction to Formic Acid: A DFT-Driven Analysis

By

Muqaddis Zahra

The ever-rising levels of emission of carbon dioxide ($CO_2$) into the atmosphere have become a significant environmental issue, causing global warming and ecological imbalance. Converting $CO_2$ into value-added chemicals through efficient catalytic routes represents a sustainable strategy to mitigate emissions while enabling carbon recycling. In this work, transition-metal-doped $B_{12}N_{12}$ nanocages are systematically investigated as single-atom catalysts (SACs) for $CO_2$ reduction to formic acid using density functional theory (DFT). Structural stability, electronic properties, charge transfer behavior, and catalytic performance of late 3d transition metals (Fe, Co, Ni, Cu, and Zn) doped on $B_{12}N_{12}$ were comprehensively analyzed by QTAIM, FMO, NBO and MEP analyses. Energetic and electronic analyses reveal that Fe, Co, and Ni form thermodynamically stable complexes with strong metal–cage interactions, whereas Cu and Zn exhibit weak physisorption. Among the studied complexes, $Co@B_{12}N_{12}$ demonstrates superior catalytic performance by simultaneously activating both $CO_2$ and $H_2$ molecules, as confirmed by adsorption energies, bond elongation and IRI analyses. The reduction of $CO_2$ on $Co@B_{12}N_{12}$ is carried out by a Langmuir Hinshelwood reaction in two competing pathways: the formate and the carboxyl pathways. In comparison of energy profiles, the carboxyl route is kinetically and thermodynamically preferable and has lower activation barriers and thermodynamically feasible reaction steps.

# Table of Contents

# List of Figures

# List of Tables

# List of Abbreviations

| | |
|---|---|
| HOMO | Highest occupied molecular orbital |
| LUMO | Lowest unoccupied molecular orbital |
| SAC | Single atom catalyst |
| TM | Transition metal |
| $G_{HL}$ | HOMO-LUMO Gap |
| 2D | Two dimensional |
| 3D | Three dimensional |
| OER | Oxygen Evolution Reaction |
| ORR | Oxygen Reduction Reaction |
| HER | Hydrogen Evolution Reaction |
| FMO | Frontier Molecular Orbitals |
| NBO | Natural Bond order |
| IRI | Interaction Region Indicator |
| QTAIM | Quantum Theory of Atoms in Molecules |
| MEP | Molecular Electrostatic Potential |

# 1 Introduction

## 1.1 $CO_2$ Emissions

Nevertheless, the main source of carbon dioxide ($CO_2$) emissions includes anthropogenic sources, with burning fossil fuels like coal, oil, natural gas, etc. Key areas of major emissions are electricity and heat generation, transportation, industrial processes (especially cement manufacturing) and changes in land use (i.e., deforestation) [1]. The current higher level of $CO_2$ concentration in the atmosphere is a result of a steep increase in $CO_2$ concentration since the pre-industrial period, where it stood at about 280ppm, to the present level of more than 420ppm, which can be attributed to human activity. Through global observations, it has been noted that the $CO_2$ emissions are rising at an annual rate of over 36 Gigatons $CO_2$ since 2010, whereas in the years before that the emission was 22 Gigatons $CO_2$ [2]. This fantastic growth in emissions is inextricably connected with growing energy consumption, industrialization, and population, which underlines the necessity to consider the relevant carbon regulation and reduction strategies.

## 1.2 Global Environmental Concerns Related to $CO_2$ Emissions

### Global Warming

Climate change fueled by global warming is one of the most significant global environmental issues that revolve around increased $CO_2$ emission. Carbon dioxide traps and releases infrared rays, which increases the greenhouse effect and causes a long-lasting rise in the average surface temperature of the earth. This warming interferes with the climatic systems, changes the precipitation, and raises the frequency of heatwaves, droughts, and other extreme weather conditions in frequency and severity. The continued increase in the level of $CO_2$ has thus become the main concern to global environmental stability and human sustainability [3].

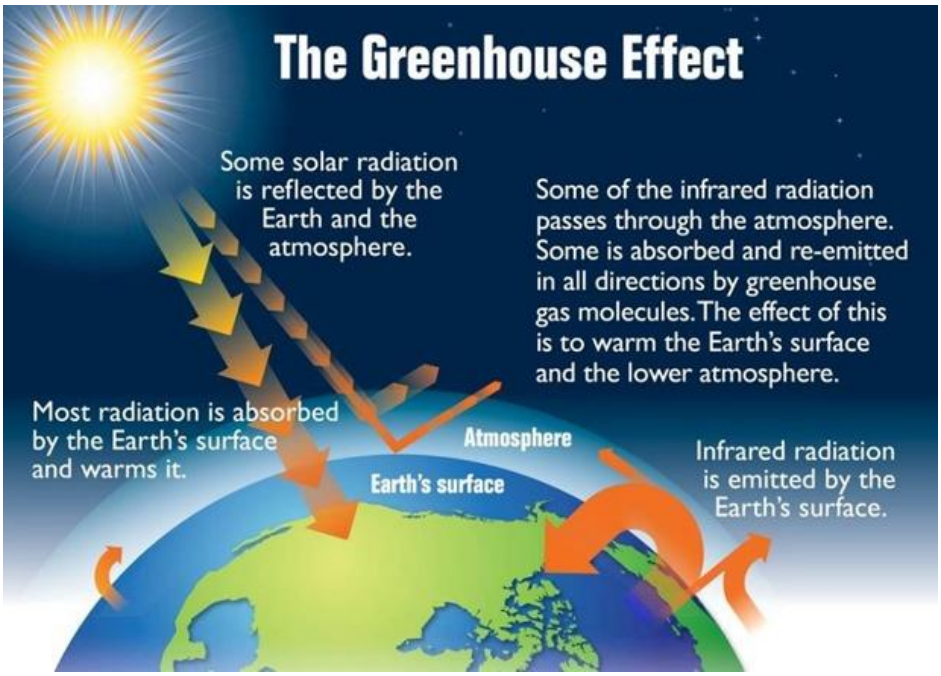


Figure 1.1 Greenhouse Effect

**Ocean Acidification**

The second significant environmental impact of high $CO_2$ emission is the acidification of the oceans caused by absorption of $CO_2$ in the atmosphere of the sea water. About one-third emitted $CO_2$ dissolves in the oceans where it reacts with water to produce carbonic acid that results in a decrease of the oceanic pH. This process of acidification has a negative impact on marine ecosystems, especially the calcifying organisms such as corals, mollusk and plankton by inhibiting their capacity to develop calcium carbonate shells and skeletal structures. Persistent $CO_2$ emission endangers marine biodiversity and interrupts food chains in the ocean which presents a major threat to fisheries and coastal living in the world [4].

**Ecosystem Degradation and Biodiversity Loss**

Increased $CO_2$ emissions also lead to the degradation and loss of biodiversity in the ecosystem by changing the habitat condition under climate conditions. Shifts in climate, rainfall, and seasonality influence the distribution of species, their migration and reproduction. There is a change in vegetation structure in the land-based ecosystems such as forests and grasslands, and sensitive species are in danger of becoming extinct given that they have a low adaptive ability.

Moreover, climatic stress caused by $CO_2$ is combined with other human pressures, including forest destruction and land use, which speeds up the disorder in ecosystems and endangers world biodiversity [5].

## 1.3 $CO_2$ as a Carbon Resource and Its Chemical Utilization

$CO_2$, with all its prominent presence in the global greenhouse gas effect, is now widely considered as a plentiful, cheap, and renewable carbon source in the production of value-added chemicals and fuels. The idea of using $CO_2$ as a C1 feedstock is a sustainable alternative to fossil carbon sources and would be in line with the global activities towards carbon neutrality. With the use of suitable catalytic methods, $CO_2$ may be converted to a variety of chemical products such as carbon monoxide, formic acid, methanol, hydrocarbons, and organic carbonates. This kind of use does not only help decrease the levels of $CO_2$ in the atmosphere but also helps bridge the anthropogenic carbon cycle through incorporation of $CO_2$ in the chemical processes in industries [6].

Nonetheless, chemical use of $CO_2$ is still a difficult task because of its thermodynamic stability and kinetic inertness which appears because of the strong C=O bonds and its complete oxidized carbon form. The conversion of $CO_2$ with high efficiency must thus utilize highly developed catalysts that can activate $CO_2$ by charge transfer, molecular bending, and stabilization of reaction intermediates [7]. New advances in catalyst systems, especially electrocatalysis, photocatalysis, and thermocatalysis have shown possible future directions in converting $CO_2$ under mild conditions. Electrochemical $CO_2$ reduction has become of great interest among them because it can be driven by renewable electricity and offers selectivity with respect to desired products, which can be tuned. As a result, this requires the creation of effective, selective, and stable catalysts to make the full potential of $CO_2$ as a viable chemical feedstock [8].

## 1.4 Importance of $CO_2$ Hydrogenation to Formic Acid

The hydrogenation of carbon dioxide to formic acid (HCOOH) has been of great interest because of its two-fold importance in the reduction of carbon and the storage of sustainable energy. Formic acid is a useful industrial chemical that has extensive applications in textile and

leather processing industries, pharmaceutical industries, and chemical production and is also efficient liquid hydrogen carrier due to its high percentage of hydrogen and the ease of storage under normal temperature conditions [9]. The transformation of $CO_2$ into formic acid is usually less energy-demanding and less electron-proton transfer steps are required than $CO_2$ to deeper products like methane or methanol, which makes it a kinetically and thermodynamically preferable pathway. In addition to that, the hydrogenation of $CO_2$ to formic acid exhibits a high product selectivity and inhibits unwanted cross reactions like the hydrogen evolution when suitable catalysts are used. As a result, this response is a good plan of action towards combining renewable hydrogen with the use of $CO_2$ and enhancing carbon-neutral chemical manufacturing and cleaner power generation systems [10].

## 1.5 Limitations of Conventional Carbon Capture Strategies

### High Energy Penalty and Economic Cost

Traditional carbon capture methods, including post-combustion amine-solvent-based carbon capture, pre-combustion and oxy-fuel combustion methods, are linked to high energy penalties. Solvents regeneration, $CO_2$ compression and purification consume a lot of power that can decrease the net efficiency of power plants by 20 to 30. The direct result of this high energy requirement is that carbon capture is economically unpromising until government policies are firmly in place or carbon prices are established. On top of this, capture units are expensive to install and maintain and hence their application is restricted especially among the developing economies [11].

### Material Degradation and Operational Challenges

Methods based on chemical absorption have a disadvantage of solvent degradation, volatility and corrosion problems. An example of such is the degradation of amines under the influence of oxygen, SOx, and NOx which results in lower capture efficiency and creation of toxic wastes. Changing solvents often, or the use of corrosive resistant materials, and complicated process control is thus a necessity that adds to the operational complexity and eventual costs. These problems make conventional capture systems less durable and less scalable to continuous operation in industry [12].

**Storage and Safety Concerns**

Many conventional methods of carbon capture are combined with geological storage (CCS), which brings the problem of the safety of long-term storage, monitoring, and possible $CO_2$ leakage. The geological formations that are suitable are geographically constrained and the long-term containment uncertainties are environmental and societal threats. In addition, underground $CO_2$ storage is still perceived negatively by the populace in most areas, which slows down the execution of the project [13].

**Lack of Value Addition and Sustainability**

The main limitation of traditional carbon capture methods is that $CO_2$ is not used as a resource but as a waste. The captured $CO_2$ cannot be used to produce an economic value and this defeats sustainability of the entire process. Conversely, the goal of carbon capture and utilization (CCU) methods is to transform $CO_2$ into fuels or chemicals, which provide an avenue to circular carbon economies. The incompatibility of the utilization pathways by the traditional capture technologies emphasizes the fact that they can do little to achieve long-term carbon neutrality [14].

**Need for Advanced Catalytic Alternatives**

These restrictions imply that the traditional carbon capture cannot be relied on to achieve climate and carbon-neutrality objectives globally. It is now becoming increasingly agreed that capture technologies should be supplemented with efficient catalytic conversion processes, which should operate under mild conditions, and allow the conversion of $CO_2$ into value-added products. This has prompted the growth of interest in catalyst-based $CO_2$ reduction strategies, such as single-atom catalysts, which are more efficient, selective, and economically viable than conventional capture-only methods [15].

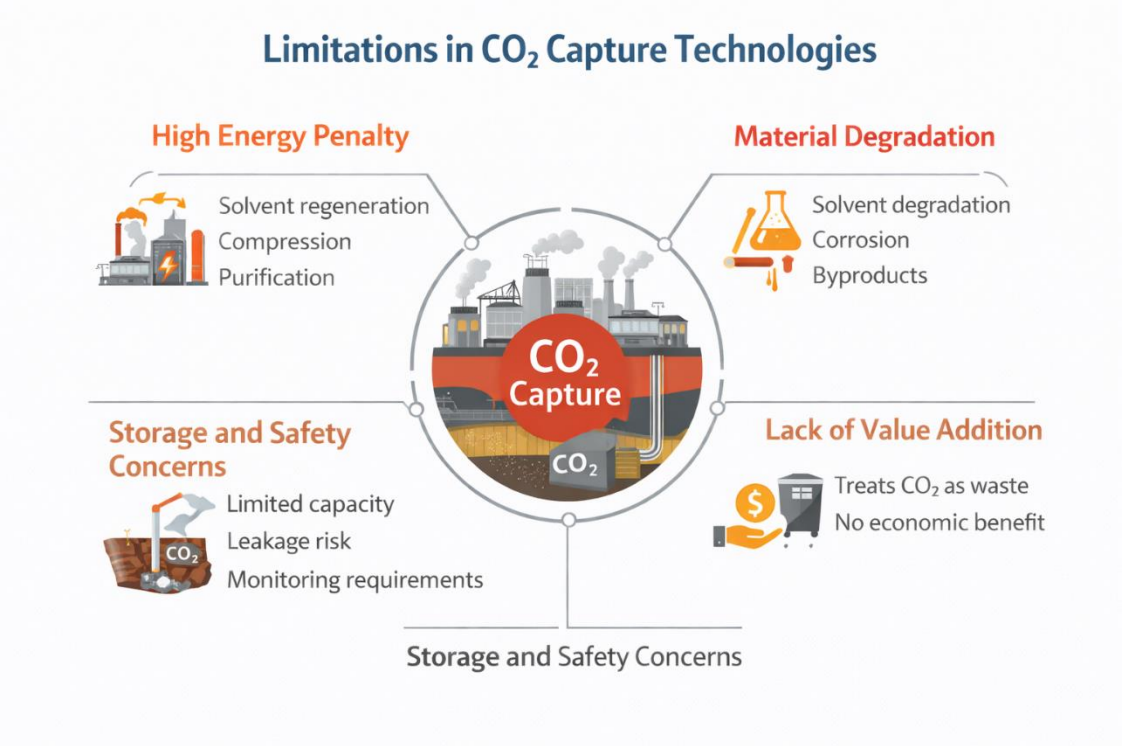


Figure 1.2 Limitations of conventional CO2 capture methods

## 1.6 Concept of $CO_2$ Reduction Reaction ($CO_2RR$)

The carbon dioxide reduction reaction ($CO_2RR$) is an electrochemical reaction whereby $CO_2$ is transformed into value-added chemicals and fuels using electrical energy usually provided by renewable sources. In $CO_2RR$, $CO_2$ molecules are adsorbed on the surface of a catalyst whereby they undergo various proton-coupled electron transfer reactions, which result in the production of reduced forms of carbon as carbon monoxide, formate, methanol, methane, and other hydrocarbons. The nature of the catalyst, electrolyte, applied potential and the reaction environment are the major determinants of the reaction pathway and final product distribution. $CO_2RR$ has attracted considerable interest because it allows the active use of $CO_2$ as a carbon feedstock and at the same time it allows us to store renewable electricity in chemical form and thus this is an attractive option to convert energy to a sustainable energy source and in recycling carbon.

## 1.7 Challenges in $CO_2RR$

### Thermodynamic Stability of $CO_2$

The $CO_2$ reduction reaction ($CO_2RR$) has several inherent challenges that impede large scale practical application despite the large amount of research done on the topic. The thermodynamic stability of the $CO_2$ molecule is high, and one of the main challenges is that the $CO_2$ molecule has strong C=O double bonds, and it is in its highest oxidation state. Consequently, the activation of $CO_2$ consumes a lot of energy, which causes high overpotentials in most catalytic systems. Such large overpotentials decrease the overall energy efficiency and make the operation costly, disfavoring $CO_2RR$ in normal conditions. Moreover, the multi-electron and multi-proton transfer steps that are associated with $CO_2$ reduction make reaction kinetics more complex and prone to side reaction [16].

### Product Selectivity

High product selectivity is another significant challenge in $CO_2RR$ because several reaction pathways occur on catalyst surfaces concurrently. The hydrogen evolution reaction (HER) can readily compete with $CO_2$ reduction in aqueous and hydrogen rich conditions because of its lower activation energy barrier, thus not selective to carbon products [17]. Numerous catalysts that are previously reported include noble metals (Au, Ag, and Pd) which are highly active in CO formation but lack selectivity in reduced products (formic acid or hydrocarbons). Equally, copper based catalysts, though have the potential to produce a wide variety of hydrocarbons,

exhibit poor selectivity and complicated product distributions, and control of the product can be difficult [7].

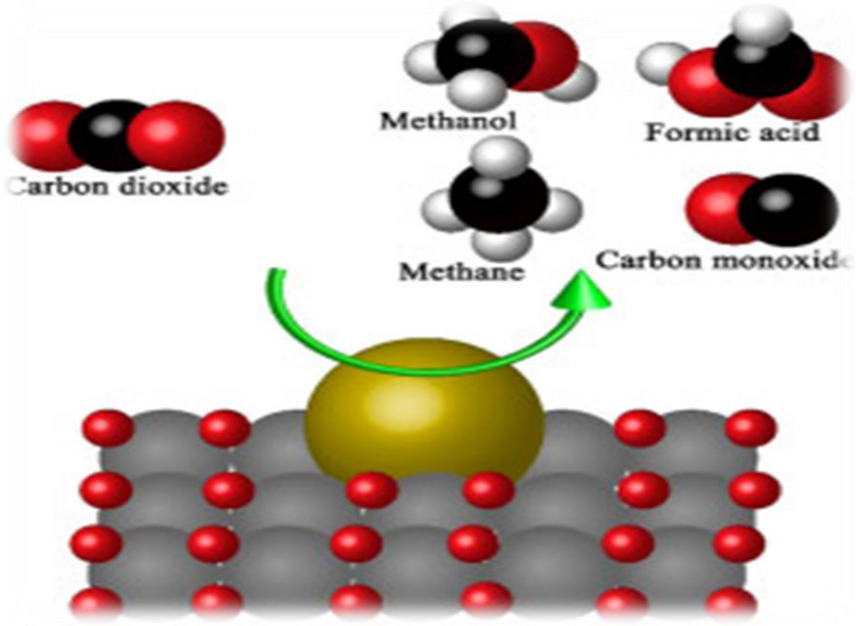


Figure 1.3 $CO_2$ reduction Products

**Catalyst Efficiency**

Also, the stability of catalysts and material productivity is an important issue. The traditional catalysts based on nanoparticles often experience a surface reconstruction, sintering, or aggregation during the reaction, which causes the loss of active surface area and the degradation of the long-term performance. Noble metals are also used as catalysts, and they are costly and scarce, thus restricting their scalability and sustainability. Further, the absence of active sites in bulk or nanoparticle catalysts make it more challenging to understand the mechanism of catalysis and thus challenging to optimize catalysts rationally. These constraints have led to the formulation of novel catalyst design concepts that would reduce the energy barrier, increase selectivity, and stability. Single-atom catalysts (SACs) in this regard have become promising alternatives because of their isolated metal active sites and adjustable electronic structures. SACs can be used to control charge transfer, stabilize key reaction intermediates and inhibit unwanted side reactions, including HER, by anchoring single metal atoms on appropriate supports. As a result, rational design of new catalysts with controlled

active sites and designed electronic properties is necessary to surmount the inherent bottlenecks of $CO_2$RR and to allow the conversion of $CO_2$ efficiently [18].

**Kinetic barriers of CO2 Reduction**

$CO_2$ is kinetically difficult to convert into value-added chemicals because the molecule is thermodynamically very stable, and its geometry is linear, leading to large activation energies to initially activate the bonds. The initial electron or hydrogen transfer reaction is commonly rate limiting, since a lot of energy is needed to distort the linear $CO_2$ molecule, and fill its antibonding orbitals. Furthermore, having multi-electron as well as multi-proton transfers during the reduction of $CO_2$ brings rival reaction routes, resulting in elevated kinetic hindrance and low selectivity of target products. The adsorption of intermediates between the reactions can also cause strong adsorption, which in turn results in an energy barrier to subsequent steps and weak adsorption, which can cause ineffective activation. Consequently, kinetic inhibitors must be overcome by means of catalysts capable of stabilizing key intermediates, reducing the activation energy of transitions, and catalyzing effective charge transfer and catalyst design is therefore one key to enhancing the velocity and efficacy of $CO_2$ conversion reactions [19].

## 1.8 Types of $CO_2$ reduction

**Electrochemical Reduction**

Electrochemical reduction of CO 2 is one of the promising methods of transforming CO 2 into fuels and chemicals with added value at the expense of electricity, preferably the renewable one. In this reaction, CO 2 is minimized at the cathode in several proton/electron transfer reagents, and the products include CO, formic acid, methanol, and hydrocarbons. It usually takes place in ambient conditions, but the reaction is kinetically demanding, as CO 2 is highly stable, and it is competing with the hydrogen evolution reaction (HER). The nature of the catalyst, the geometry of the active site, and the adsorption strength of crucial intermediates are of strong importance in product selectivity and overpotential. Consequently, the design of electrocatalysts is essential in reducing energy barriers and achieving selectivity to desired products [20].

### Thermo-catalytic Reduction

The thermo-catalytic CO 2 reduction is the hydrogenation of the CO 2 at high temperatures and pressures, usually the molecular hydrogen is employed as the reducing agent. Popular reactions are the reverse watergas shift (RWWS), methanation, and formic acid production. Under this method, catalysts reduce activation energies required in adsorbing CO 2, bond activation, and dissociation of hydrogen. Even though thermo-catalytic pathways are industrially developed, they tend to be harsh in nature and lowly selective because of the competing reaction pathways. Thus, the development of catalysts is focused on the creation of an active and selective reaction at conditions of lower activity by refining the interactions between metals and supports, as well as reaction pathways, including LangmuirHinshelwood or EleyRideal [21].

### Photo-catalytic Reduction

Photocatalytic reduction of CO 2 involves the use of solar energy to catalyze the process of converting CO 2 into fuels and chemicals using the input of photo-excited charge carriers. When a semiconductor photocatalyst is subjected to light irradiation, the electrons are excited to the conduction band of the material, and CO 2 reduction reactions are facilitated at the catalyst surface. It has a long-term solution to the problem of CO 2 conversion; nevertheless, the method is constrained by low quantum efficiency, rapid charge recombination, and low light absorption. To achieve a successful photocatalyst design, the band gap alignment, the separation of charges, and the adsorption of CO 2 and reaction intermediates should be effective. Nevertheless, it has not eliminated photocatalytic CO 2 reduction as a strategy of solar-to-chemical energy conversion [22].

## 1.9 Catalysis

The concept of catalysis was introduced by the Swedish chemist Jons Jakob Berzelius in 1835 and later given a clear and formal definition by Wilhelm Ostwald in 1894. Ostwald defines catalysis as the increase in velocity of a chemical reaction by a foreign substance, called catalyst, lowering the activation energy by reacting with the reactant molecules. Notably, the catalyst is not consumed in the reaction, and thus, it is able to enhance the transformation of many reactant molecules despite being present in low (catalytic) concentrations. Catalysis can be categorized on a broad basis of the physical condition of reactants and catalysts as either

homogeneous or heterogeneous. In homogeneous catalysis, the catalyst and reactants are in the same phase and thus, it is difficult to separate and recover catalysts. Conversely, in heterogeneous catalysis catalysts and reactants are in different phases, which has benefits of superior stability, provided easy separation, and greater practical use than with homogeneous systems. [23].

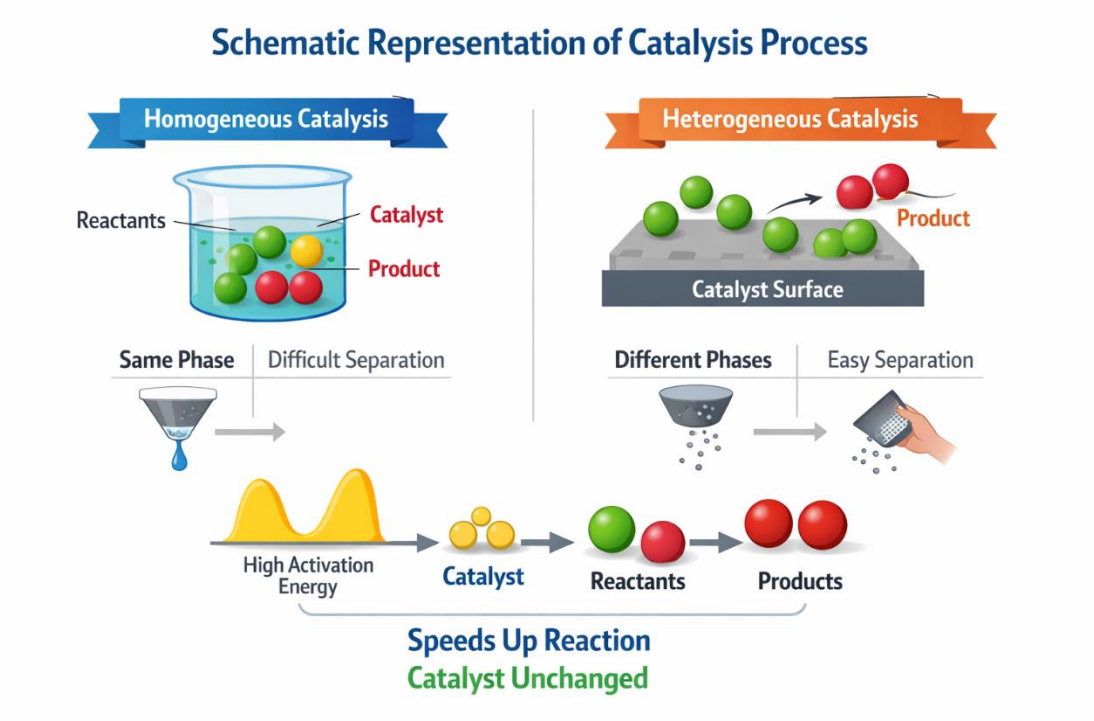


Figure 1.4 schematic diagram of catalysis

When a reaction in the absence of catalysts is slower, less selective and specific than catalyzed reaction, the control is largely dominated by the character of the active site of the catalyst and its interactions with the reactant, transition state, and product [24].

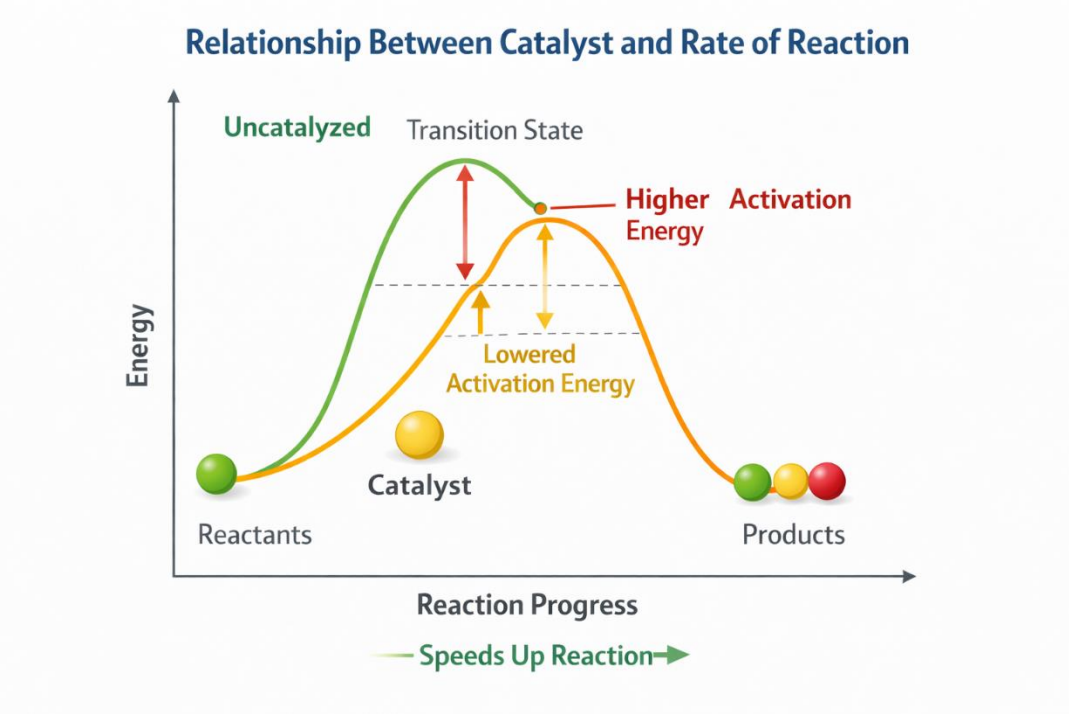


Figure 1.5 Relation between Rate of reaction and Catalyst

In the recent past, there have been wide efforts into the development of heterogeneous electrocatalysts made of non-precious transition metals in the form of phosphides, oxides, and nitrides, including Co, Ni, Mo, and Fe, in addition to their derivatives; however, their catalytic activities are relatively low. Single-atom catalysts (SACs) have received much interest in contrast because of their remarkable features, especially high selectivity and maximized use of each metal atom, but they are potentially good alternatives to efficient electrocatalysis [25].

Active metal particles are being decreased to increasingly smaller sizes, nano-, sub-nanometer, and finally, atomic sizes to increase the efficiency of atomic utilization. Since molecular and atomic catalytic reactions require accurate atomic-level structure control, single-atom catalysis offers an effective platform to study and conceptualize these basic catalytic reactions [26].

## 1.10 Single Atom Catalysts (SACs)

Catalysis has become one of the most widely used because of its low cost and high efficiency. studied field in science. Natural sources like methane gas, oil, coal, etc. are converted to oil products through the process of catalysis. solar energy and biomass may be converted to usable energy, and at the same time. producing useful chemical substances. Since 85% of chemical

production is dependent on catalytic processes, there is need to discover highly efficient catalysts [27].

The most common type of supported metal catalysts is the noble metal-based (Rh, Pd, Pt, Ru, Au, and Ag) type, which is commonly employed in catalysis but due to their high cost and scarcity, are not very practical on a large scale. In traditional nanoparticle catalysts, all atoms are catalytically active on the surface, with a large portion of atoms in the particle core being inactive and, hence, not utilized as catalysts, such as only 50 percent of atoms being catalytically active in 2 nm nanoparticles. Even though the smaller the particle size, the higher the number of active surface atoms and the intensity of metal-support interactions and quantum size effects, the best approach to maximizing utilization of the metal is single-atom catalysis (SAC). SACs can be dispersed on appropriate supports to obtain near-perfect atomic efficiency, better selectivity and improved catalytic activity, which makes them a highly promising alternative to traditional supported metal catalysts [28]. The first study of single-atom catalysis on isolated metal atoms on FeO surface was reported by Zhang Tao and co-workers in 2011. Single-atom catalysts are highly stable, highly utilized with metals and can be tuned in terms of composition compared to conventional heterogeneous catalysts. The individual dispersion of the metal atoms on appropriate support maximizes the supply of active sites and results in higher catalytic activity and efficiency [29].

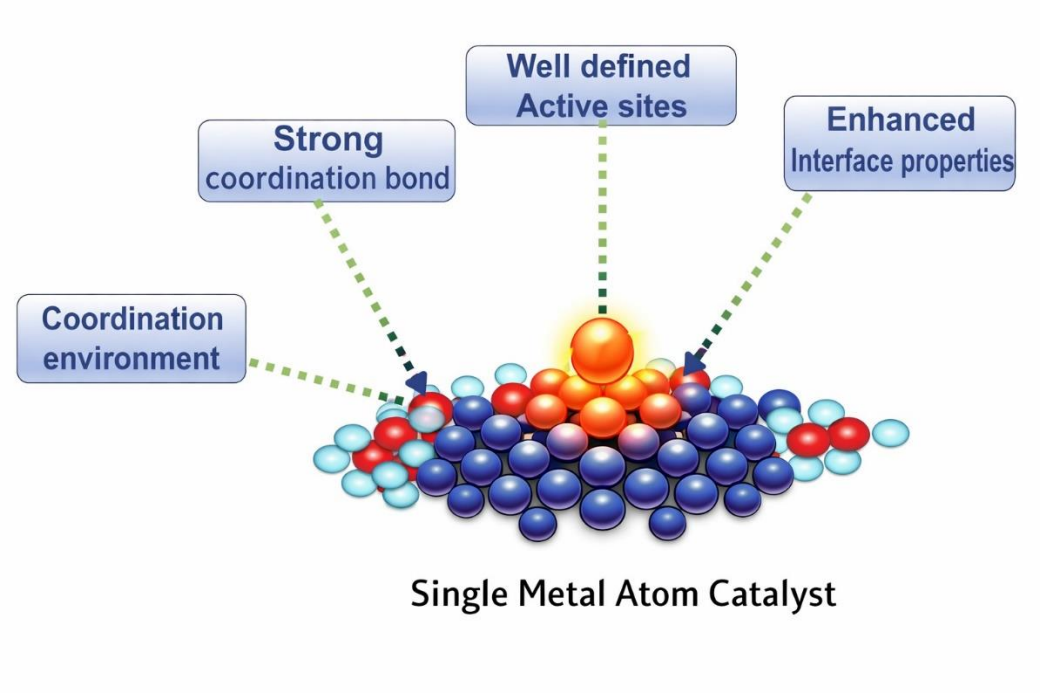


Figure 1.6 Properties of SACs

It has also been shown that single-atom catalysts exhibit excellent electrocatalytic efficiency in a broad variety of electrochemical reactions, including nitrogen reduction [30], oxygen evolution [31], oxygen reduction [32], $CO_2$ reduction [33], and hydrogen evolution [34]. Single atoms being used as active sites in single-atom catalysts offer very clear and consistent adsorption sites with which they offer more structural clarity in comparison to supported metal nanoparticles or cluster catalysts [35].

## 1.11 Synthesis of Single Atom Catalysts (SACs)

The isolation of single crystal atoms on suitable support materials is the synthesis of single-atom catalysts (SACs). The dispersion rate of such high dispersion is not easy since the metal atoms are more likely to migrate to become cluster when conducting the synthesis or post-treatment. Thus, the preparation conditions and choice of the appropriate strategies of synthesis should be carefully controlled to stabilize single metal atoms and produce successful SACs with well-definite active sites.

**Mass Selected Soft-landing Technique**

The advanced technique employed in the synthesis of metal clusters is the mass-selected soft-landing technique, which allows the synthesis of metal clusters at a specific atomic composition and therefore this is highly promising in the synthesis of single-atom catalysts (SACs). This method also offers a perfect system of examining the interactions between metals and supports at the atomic level using model systems that are well defined. The clusters of metal or metal nanoparticles in this technique are produced in the gas phase initially by laser ablation, gas-phase condensation or chemical synthesis. These formed clusters are then ionized, usually given a positive charge, and sent through a mass spectrometer where the ones of the chosen mass are selectively separated out. Lastly, the selected species is massively deposited and then carefully deposited onto an appropriate substrate through controlled deposition process, allowing the creation of isolated metal atom/clusters with limited aggregation [36].

**Atomic Layer Deposition**

Atomic Layer Deposition (ALD) is an excellent method of producing model catalysts as well as investigating the impact of particle size, support-surface characteristics, and overlayer structures on metal or alloy nanoparticles. The technique is important in the study of catalytic mechanisms because it enables a discrete control of the character of catalysts including their size, shape, dispersion, and metal loading. The precursor molecules in ALD are added through the reaction chamber in a cascade fashion with the precursor interacting with the substrate surface in a self-limiting fashion to produce a monolayer. Unutilized precursors and byproducts are eliminated and preceded with the next precursor. The repetition of this cyclic reaction allows an accurate growth of materials at the atomic level and in the desired thickness of the film [37].

**Wet chemistry Method**

Wet chemistry technique is a straightforward and readily available technique, which can be performed in regular laboratories, and thus is applicable when the scale of synthesis is large and industrial synthetic supported metal catalysts are desired. The purpose of this technique is

to avoid aggregation of metal species either during the synthesis process or even after treatment due to the chemical fixation of metal complexes on appropriate supports. Wet chemical methods have conventionally been applied to the preparation of single-atom catalysts (SACs) because single-metal atoms are already in the starting materials, so they provide a convenient and scalable synthesis plan [38].

## 1.12 Supports for Single Atom Catalysts

The control of the catalytic activity of single-atom catalysts depends on the choice and modification of the appropriate support material. The aggregation of isolated metal atoms can be suppressed by appropriate support to unfavorable environments in which clustering will occur; hence, the sites occupied by single atoms can be stabilized. Besides, the first coordination condition formed by the support has a significant impact on the electronic structure and reactivity of individual metal atoms. Hence, the interaction between the support materials and the metal atoms must be comprehended and optimized to improve the catalytic activity of single atoms catalysts.

**Different Supports for Single-Atom Catalysis**

The activity of single-atom catalysts (SACs) is highly dependent on the type of support material that has a significant role in stabilizing isolated metal atoms and manipulating their electronic structure. The two popular types of supports that have been studied extensively concerning SACs are two-dimensional (2D) sheets and cage-like nanostructures. Graphene, nitrogen-doped graphene [39], carbon nitride (g-$C_3N_4$) [40] and hexagonal boron nitride (h-BN) [41] sheets are 2D materials that have been widely used because of their large surface area, good conductivity and availability of heteroatom anchoring sites that inhibit metal aggregation. Strong metal support interactions are facilitated by these sheet-based supports, to form well-defined active sites and increase catalytic activity. Several cage-like nanostructures were investigated as effective in stabilizing individual metal atoms. A prominent one is carbon-based fullerenes ($C_{60}$), which offer a restricted three-dimensional framework and intense interactions between the metal and the cage, preventing aggregation of the metal. Theoretical and experimental studies have focused on transition-metal-doped $C_{60}$ cages to use in catalysis, gas adsorption, and electronic modulation [42][43].

Inorganic nanocages like $Al_{12}N_{12}$ and $Al_{12}P_{12}$ are other significant classes and structurally like $B_{12}N_{12}$ but have a high level of polarity and discrete coordination environment. These cages have been stated as bright prospects of anchoring individual metal atoms providing greater stability, charge transfer, as well as catalytic conductivity regarding small-molecule catalysis, such as $CO_2$ and $H_2$. These cage-based systems offer alternative cage platforms to boron nitride nanocages on which to conduct single atom catalysis and are also becoming the focus of theoretical catalyst design [44].

## 1.13 Location of Metal Atom on Support

The smaller the metal size, the greater the surface free energy leading to highly active sites that react intensely with support and adsorbates. Therefore, to explain the reactivity and behavior of metal nano-catalysts comprehensively, one should understand size effects [45]. In the single-atom catalysts, the chemical potential of the constituent metals determines the location of individual atoms of the elements on the supports. Indicatively, in palladium-gold systems, higher-chemical potential gold atoms are found exclusively at corner sites, whereas in graphene-based SACs, and higher-chemical potential atoms are isolated metal atoms that are anchored by carbon vacancy defects [46].

## 1.14 Metals Used in SACs

The use of noble metals, such as platinum and palladium, has been quite popular because of their outstanding characteristics in catalysis in producing and converting energy based on their electronic and surface characteristics. All these properties make them very efficient catalysts in various chemical and electrochemical reactions. Natural resources of noble metals are, however, very limited, having a composition of less than 3 wt.% of the total resources present on the earth. Their high cost and low concentration in the market contribute greatly to their unavailability in large quantities and their inability to practical application as catalysts because of this scarcity, thus compelling the quest to find other inexpensive catalyst systems with similar functionality [47]. Scientists are exploring alternative catalysts and innovative approaches to resolve the challenges of constraint of their availability and cost associated with the scarcity of Pt and Pd. Various types of metals have been studied as active sites in single-

atom catalysts (SACs), based on the desired reaction and desired catalytic characteristics. Some of the most common SAC metals used are transition metals like Fe, Co, Ni, Cu, Mn and Zn because they have partially filled d orbital which enhance strong interactions with the reactant molecules and allow effective transfer of charge to take place. The metals play a crucial role, especially due to their relatively low costs and tunable electronic structures, which enable them to be used in reactions like $CO_2$ reduction, hydrogen evolution, oxygen reduction and nitrogen fixation [48].

## 1.15 Applications of SACs

The SACs have received a lot of attention because of their superior catalytic activity in the broad variety of chemical and energy-related reactions. SACs have atomically dispersed active sites, which allow them to possess maximum utilization of metals, clearly defined coordination environments, and tunable electronic properties, which make them very efficient in energy conversion and storage reactions [49]. Famous examples are $CO_2$ separation, with SACs demonstrating a greater selectivity towards value-added products like formic acid and carbon monoxide; hydrogen evolution and oxygen evolution reactions (HER/OER) in water splitting [50]; and oxygen reduction reaction (ORR) in fuel cells. SACs have also been found to be highly active in nitrogen reduction reactions (NRR) to produce ammonia, other traditional methods of heterogeneous catalysis, such as CO oxidation, selective hydrogenation, and oxidation reactions. Moreover, SACs are highly stable and sinter resistant and thus have potential for long-term catalytic performance. The versatile applications of these types of SACs make them the next generation of catalysts used in sustainable energy technologies and green chemistry processes[51].

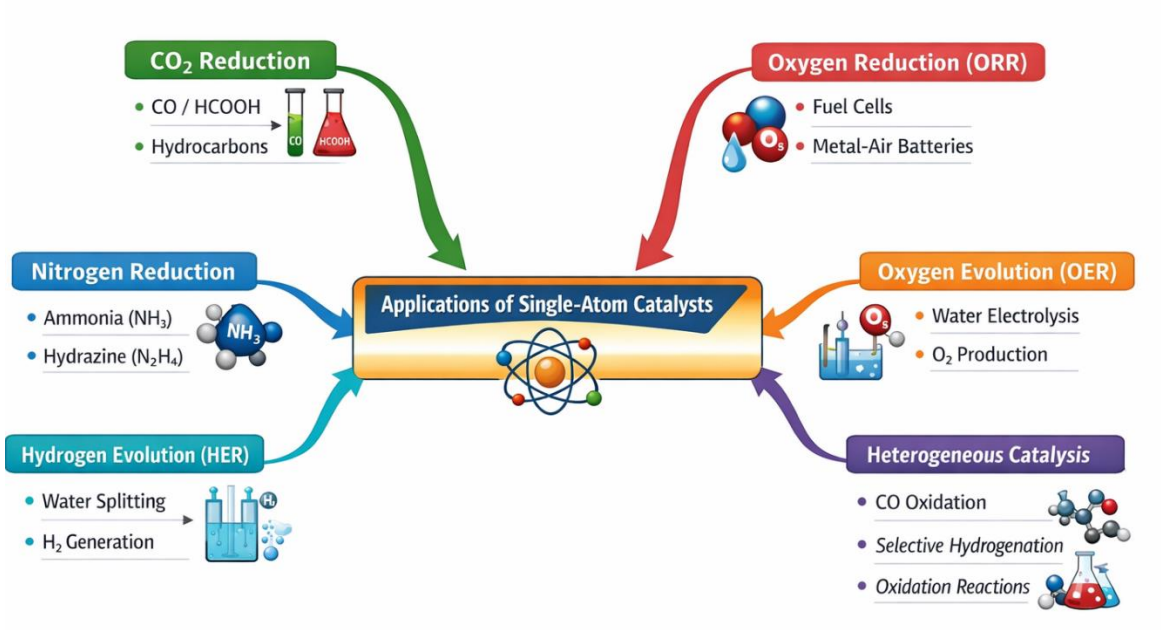


Figure 1.7 Applications of SACs

## 1.16 $B_{12}N_{12}$ Nanocages as Efficient Catalyst Supports

The nanocages of $B_{12}N_{12}$ have proven to be most promising in single-atom catalysis because of its exceptional structural and electronic features. $B_{12}N_{12}$ cage is made up of an alternating sequence of boron and nitrogen atoms in closed, highly symmetrical cage that comprises of eight hexagonal and six tetragonal rings [52]. Several sites with low coordination, especially boron-containing areas with electron-deficiency character, are also available in this geometry and are strong anchors to isolated metal atoms. The availability of the p-orbitals of boron leads to an efficient interaction between the metal and support via charge transfer and coordination bonding to avoid aggregation of metal atoms and promote high stability of catalysts [53]. Moreover, $B_{12}N_{12}$ nanocages are highly stable thermally, chemically and oxidation resistant and thus they can be used in extreme catalytic environments. These materials, due to their peculiarities, can be used in several applications such as gases storage, catalysis, drug delivery, and optoelectronics [54]. All these properties, structural strength, tunable electronics, and powerful metal anchoring properties, have made $B_{12}N_{12}$ nanocages the most efficient and reliable support of single-atom catalysts, especially during $CO_2$ activation and reduction reactions [55].

## 1.17 Transition Metal Doping

Transition metal-doped $B_{12}N_{12}$ nanocages are selected for this study and previous studies showed that doping significantly alters their properties. Mn shows the best affinity to the $B_{12}N_{12}$ nanocage and Zn shows the least affinity. The ideal doping site is the B-64 which is the site between the hexagonal and tetragonal rings. According to the density of states (DOS) analysis, doping decreases the HOMO-LUMO band gap, which increases the metallic nature of the nanocage [56]. TM doping dramatically changes the electronic characteristics of the $B_{12}N_{12}$ nanocages, lowering the energy gap. Electronic chemical potential, electronegativity, chemical hardness, electrophilicity, chemical softness, NBO charge, and density of states are some of the observed properties that change significantly upon adsorption of the pristine $B_{12}N_{12}$ [57]. Such changes render TM-doped $B_{12}N_{12}$ nanocages as potential candidates to be utilized in hydrogen storage and sensing [54]. $B_{12}N_{12}$ nanocages doped by transition metals have the capability of boosting $CO_2$ adsorption and activation by charge transfer and π-backdonation. TM doping reduces the energy activation barrier, which guides $CO_2$ reduction to formic acid. They are stable catalysts, redox adaptable, and promising catalysts of $CO_2$ reduction.

## 1.18 Problem statement

Previously used catalysts like metal nanoparticles (e.g., Au, Pd, and Pt) and metal-organic frameworks (MOFs) for $CO_2$ reduction to formic acid had had problems such as poor selectivity, agglomeration, low access to active sites and high activation energy barrier leading to inefficient catalysis. These disadvantages highlighted the importance of more studies that could enhance the efficiency of these materials in the reaction of reducing $CO_2$. Conversely, transition-metal-doped $B_{12}N_{12}$ nanocages overcome these problems through their high structural stability, excellent dispersion of active metal sites, and enhanced $CO_2$ adsorption due to their porous structure. This ensures efficient electron transfer and selective reduction to formic acid while maintaining durability under reaction conditions.

## 1.19 Objectives

- To explore doping mechanism of first row TMs on $B_{12}N_{12}$ to design SACs.

- To investigate structural and electronic properties of TM doped $B_{12}N_{12}$.
- To evaluate catalytic property of TM doped $B_{12}N_{12}$ for $CO_2$ reduction to formic acid.

## 1.20 Motivation

Single atom catalysis is an advanced area in field of research because it shows enhanced reactivity towards chemical reactions. $CO_2$ reduction reactions are important reactions for conversion of $CO_2$ into useful products. Transition-metal-doped $B_{12}N_{12}$ nanocages have high structural stability, excellent dispersion of active metal sites, reaction selectivity and due to this, it is anticipated that it will be more efficient in $CO_2$ reduction.

# 2 Literature Review

**Sajjad Ali et al.** investigated defective and doped graphene, specifically graphene with a monovacancy (m-VacG), as a support for single-atom catalysts (SACs) in $CO_2$ hydrogenation to formic acid. Cu, Pd, and Ru atoms on m-VacG were identified as stable SACs due to their high adsorption energies surpassing the cohesive energies of their bulk forms. Two reaction pathways were explored: Path A, starting with coadsorption of $H_2$ and $CO_2$, and Path B, initiated by $H_2$ adsorption. Path B was thermodynamically favorable, with a lower energy barrier. Among the catalysts, Pd/m-VacG exhibited the highest catalytic activity, demonstrating the lowest energy barrier, making it a promising candidate for efficient $CO_2$ conversion [58].

Using Density Functional Theory, **Guanming Chen et al.** investigated single-atom (SACs) and dual-atom catalysts (DACs) on $SnS_2$ monolayers for $CO_2$ electrochemical reduction ($CO_2RR$) to formic acid. Sn-SACs were very efficient and selective in the production of formic acid with low limiting potential of -0.29 V. Stability test showed that low metal coverage and separated metal centers in catalysts are synthetically viable. Bader charge and electronic structure calculations revealed that $SnS_2$ substrate promotes CO 2 reduction provision of the electronic charge. The research notes that $SnS_2$-based SACs are some of the potential candidates towards sustainable $CO_2$ recycling [59].

**Dr. Dusan et al.** assessed Ru and Cu atoms integrated into defected graphene (Ru-dG and Cu-dG) as single-atom catalysts (SACs) to convert $CO_2$ to formic acid (FA) using a density functional theory (DFT). As opposed to traditional catalysts, SACs guarantee each metal atom is active. A total of three pathways were examined, and the direct one was excluded based on high energy barriers (>35 kcal/mol). Ru-dG catalyzed the hydrogenation of $CO_2$ with dissociated $H_2$, whereas Cu-dG used co-adsorbed $H_2$ protons. Both had low activation energies (<20 kcal/mol), with Ru-dG being more stable, as it did not destabilize under the reaction conditions. Cu-dG had reduced binding stability, and this restricted its activity. Ru-dG is an effective SAC in the reduction of $CO_2$ to FA [60].

**Mehdi D. Esrafili et al.** examined the $CO_2$ hydrogenation on a single Co atom on nitrogen-doped graphene ($CoN_3$-Gr) with dispersion-corrected density functional theory. Strong Co-3d

and N-2p hybridization stabilizes the Co atom on the defective nitrogen-doped graphene, and the diffusion barriers are high, which makes the structure stable. The Co atom is positively charged to allow the activation of $H_2$ and $CO_2$, and a formate (HCOO) intermediate with a low activation energy of 0.31eV was formed, which allowed the reaction to occur at room temperature. The energy barrier needed to convert to HCOOH is manageable at 0.51 eV, whereas there is no likelihood of side product formation because the energy barrier is higher. The paper identifies $CoN_3$ -Gr as a high-activity and selective catalyst in the efficient conversion of $CO_2$ to hydrogenation [61].

**Wei Xun et al.** performed first-principles calculations on electroreduction of $CO_2$ on transition-metal atoms (Sc, Ti, Fe, Co, Ni) on $MoSi_2N_4$ monolayers. Tunable selectivity and pathways were observed in the catalysts through tuning of the d-band properties. Co@$MoSi_2N_4$ preferred HCOOH formation at 0.89 eV barrier, whereas the others formed $CH_4$ at low barriers of 0.811.24 eV. $MoSi_2N_4$ greatly improves the stability of the air, which increases its usefulness, and these catalysts have potential to reduce $CO_2$ effectively in the context of a renewable energy source [62].

**Zhao et al.** examined single-atom catalysts, which include transition-metal atoms (TM) decorated by $Na_4SiMo_{12}$) in reducing $CO_2$ by the use of DFT. Sc, Cr, Mn, Ti, and V catalysts were highly stable and active, with Cr@$Na_4SiMo_{12}$ having a low limiting potential of -0.23 V to HCOOH formation and $Na_4SiMo_{12}$ having high selectivity (UL = -0.48 V). Polyoxometalates (POMs) were considered as electron sponges, which promoted electron transfer. According to the study, TM@ $Na_4SiMo_{12}$ has potential as catalysts in reducing $CO_2$ technologies [63].

**Tianfu Liu et al.** investigated the electrochemical $CO_2$ reduction of single-atom catalysts, which are based on graphdiyne, through DFT. Co–graphdiyne was the most active and selective Mn, Fe, Co, Ni, Cu, and Zn SACs that generate methanol with an energy barrier of 0.31 eV. The paper has highlighted the importance of the d-band center, metal atomic number and sp-hybridization in catalytic performance and selectivity [64].

**Liu et al.** explored the use of defective boron nitride fullerenes anchored by transition-metal atoms (TM) to reduce $CO_2$ by means of DFT. Mn-$B_{23}N_{24}$ and Fe- $B_{23}N_{24}$ were highly active

and selective in the production of $CH_4$ and depended on the binding energy of intermediates of the reaction i.e. CO and OH. The curved structure, characterized by a pyramidalization angle of about 26, had a great enhancing effect on performance, but TM-$N_3$ centers were the best. B defects were more effective than N defects. Limiting potential decreased to -0.25 V with curved fullerenes as opposed to -0.64 V with flat BN sheets and the curvature effect was observed to provide greater efficiency. The current research novelty makes curved TM-doped BN fullerenes as a promising $CO_2$RR catalyst [65].

**Zhang et al.** made palladium (Pd) nanoparticles on the hierarchical nitrogen-doped carbon nanocages (Pd/hNCNCs) to be efficient in reducing $CO_2$ to formate. The catalyst had a Faradaic efficiency of more than 95 percent and a high formate current density of 10.3 mA per cm -2 at -0.25 V. This is due to the homogenous size Pd nanoparticles, N-doped support to enhance intermediate adsorption and better mass/charge transfer through the hierarchical structure. The research provides a direction of developing efficient electrocatalysts to convert energy [66].

**Zhou et al.** examined the vanadium-doped silicon clusters (VSin, n: 12-15) to evaluate the ability of these clusters in hydrogenating $CO_2$ to C 1 products using ab initio calculations. The kinetic barrier in these clusters varied in 0.67 to 1.53 eV, and the selectivity was dependent on the geometry and size of the cluster. They can be prepared with the high stability and capture light in the visible to ultraviolet spectrum and thus can be used to convert $CO_2$ photo catalytically. The catalytic activity of the high level is attributed to unsaturated states of the Si cage, sp-d hybridization, and V-Si charge transfer which provide information on how to design silicon-based nanocatalysts in renewable energy [67].

**Zhang et al.** studied $CO_2$ hydrogenation to formic acid (HCOOH) using a single nickel (Ni) atom on O-vacancy defected $Ti_3C_2O_2$ (Ni@$Ti_3C_2O_2$) through first-principles calculations. The Ni atom was stably anchored, and the reaction proceeded via a low-energy pathway with a barrier of 0.54 eV. Low barrier of 0.12 eV facilitated easy desorption of HCOOH, providing effective hydrogenation. High barriers for side reactions revealed the catalyst's selectivity for synthesis of HCOOH. This paper clarifies $CO_2$ hydrogenation processes and emphasizes the possibilities of Ni@$Ti_3C_2$ for $CO_2$ fixation [68].

**Kan Homlamai et al.** used DFT calculations to investigate non-noble metal single-atom catalysts (SACs) comprising Fe, Co, Ni, and Cu supported on graphitic carbon nitride ($gC_3N_4$) for $CO_2$ hydrogenation to formic acid. Being adsorption energies ranging from −0.16 to −0.40 eV, Fe-$gC_3N_4$ displayed the best $CO_2$ adsorption stability. A two-step reaction mechanism was proposed, with the catalytic activity order being Fe-$gC_3N_4$ > Co-$gC_3N_4$ > Cu-$gC_3N_4$ > Ni-$gC_3N_4$. The research explains the importance of non-noble metals in $CO_2$ adsorption and hydrogenation, hence leading catalyst design [69].

**Mehdi D. Esrafili et al.** performed DFT calculations to examine Ti-doped graphene nanoflake (Ti-GNF) as a catalyst for $CO_2$ reduction to generate formic acid via hydrogenation. The results revealed that the significant positive charge on the Ti atom improves the surface reactivity of the graphene nanoflake, therefore enabling the catalytic process. The calculated activation energies suggest that Ti-GNF has a massive potential in converting $CO_2$ to formic acid because it is a good catalyst [70].

**Ge Yan et al.** examined $CO_2$ to formic acid hydrogenation $Pt_4$/SV catalyst, which is composed of a platinum -based $Pt_4$ cluster doped with a single vacancy, to overcome the cost and scarcity of platinum. DFT computations were performed on four reaction pathways, where TER was found to be the most dominant. $Pt_4$/SV was very stable and active, and the activation energy was minimum 0.56eV. The research emphasizes the potential of $Pt_4$/SV and provides information about $CO_2$ reduction technology and platinum-based catalysts [71].

**J. Sirijaraensre et al.** have studied Cu impregnated in graphene (Cu/dG) to hydrogenate $CO_2$ to formic acid by DFT. Cu/dG does the adsorption and heterolytic cleavage of $H_2$ to make Cu-H on hydrogenated graphene, which can easily react with $CO_2$ to produce protonated $CO_2$. Nonetheless, in the absence of an adequate amount of $H_2$, the catalytic reaction is blocked by the formation of copper-formate, which entails high-energy consumption during the conversion of FA. The paper highlights the significance of $H_2$ in facilitating conversion of copper-formate to formic acid [72].

**Abdulrahman et al.** explored the use of $Fe_1$-$B_{12}N_{12}$ as a noble-metal-free single-atom catalyst (SAC) to reduce the electrochemical $CO_2$ reduction using DFT. The Fe atom has a strong binding affinity with the $B_{12}N_{12}$ nanocage and the interaction energy is -1.34 eV and is very

stable and can be dispersed well. Fe doping improves the electrical conductivity of the nanocage considerably by decreasing the band gap of the pristine nanocage (6.86 eV to 4.20 eV) to ensure the transfer of electrons during catalysis. Efficient conversion of $CO_2$ to $CH_4$ and $H_2O$ is observed in mechanistic analysis, and the calculated overpotentials are 1.00 V in the COOH and 0.92 V in the HCOO pathways. Overall, $Fe_1$-$B_{12}N_{12}$ has become an effective and feasible SAC to reduce $CO_2$, to provide a feasible pathway of reducing greenhouse gases [73].

According to **Yongcai et al.**, CO was obtained as the major product at relatively low negative potentials during electrochemical reduction of $CO_2$. As CO is a major intermediate towards further production of methanol and C-C coupling reaction, efficient catalyst should have a high CO adsorption capacity. Theoretical studies grounded on the Cu-$N_4$-C model suggested that the carboxylation of $CO_2$ reacts with a high energy barrier and preferential to produce formic acid but with low CO adsorption. Since there were a lot of N–H bonds involved in the process of not only synthesizing N-doped graphene but also in the electrocatalytic reduction process, a model of the structure was suggested by Yongcai et al. It was a CuN4HC structure. The simulations of the ab initio molecular dynamics showed that this arrangement is thermally stable at 600 K to at least 3 ps. The Cu-$N_4$H-C model has the advantage of having the partial reduction of the Cu + center, which improves the CO adsorption and decreases the energy barrier of $CO_2$ carboxylation to 0.23 eV with the energy barrier of methanol formation being lowered to 0.50 eV. Moreover, potassium doping also enhances further the reduction of catalysts and the efficiency of $CO_2$ to HCOOH reaction. Altogether, this work illustrates that local microenvironmental modulation of single Cu atoms is a very important factor in regulating the $CO_2$ reduction pathways and offers valuable information on how to design high-performance single-atom catalysts [74].

In a study, **Jing Shen et al.** investigated the electrochemical reduction of $CO_2$ by cobalt porphyrin complexes by density functional theory (DFT) calculations to develop a mechanistic understanding of the catalyst behavior. They find that $CO_2$ reduction is an attractive pathway to afford renewable energy as fuels and chemicals, but that its efficiency is too low and applicability remains restricted by overpotential. The authors determined the $CO_2^-$ anion adduct as one of the major reaction intermediates, and the reaction intermediate is only formed when the cobalt center is reduced to the Co(I) oxidation state. The reaction pathway diagram

indicates that CO was the major product, which was produced through a decoupled proton-electron transfer reaction. Formic acid, on the other hand, is produced as a minor product via an intermediate [Co(P)–(OCHO)], and methane is produced by reduction of the CO to produce a series of proton-coupled electron transfer reactions. Overall, the theory results are consistent with the experimental data and further explain the reaction mechanism of $CO_2$ reduction on the cobalt-based molecular catalysts that can be used as a strong guiding principle of designing more effective $CO_2$ reduction catalysts [75].

A detailed DFT study of the $CO_2$ reduction by a new dual-chromium anchored tri-vacancy 12 borophene ($Cr_2$ /TV-$\beta_{12}$) electrocatalyst was reported by **Naval et al.** To create an 11-membered ring structure in 3-vacancy $\beta_{12}$-borophene, a tri-vacancy defect was then introduced and the systematic doping of 3-vacancy $\beta_{12}$-borophene with different transition metals (Co, Cr, Cu, Fe, Mn, Ni, and Zn) was performed in their study. Out of 28 configurations that were studied, $Cr_2$ /TV-$\beta_{12}$ was found to be amazingly stable, with good adsorption capacity of $CO_2$ and efficient molecular activation as validated by PDOS, charge density difference, Bader charge and COHP. The catalyst was highly selective to the reduction of $CO_2$ with a low limiting potential of -0.45 V, whereas the catalyst was also very suppressive to the competing hydrogen evolution reaction (HER) which had a higher limiting potential of 0.57 V. Formaldehyde was found to be the major reaction product, and the catalyst was also very resistant to CO poisoning. Overall, the research demonstrates the high promise of dual-atom-doped defective borophene as a highly selective and efficient electrocatalyst in the $CO_2$ reduction reaction [76].

A density functional theory (DFT) study by **Chen Guo et al.** was aimed at investigating the electrocatalytic reduction of $CO_2$ to $C_1$ products (CO, HCOOH, $CH_3OH$, and $CH_4$) on g-$C_3N_4$ frameworks modified with single Ni, Co, and Fe atoms. Their findings indicated that the isolated metal atoms have some preference in occupying the edge to center positions of the g-$C_3N_4$ cavity. Analysis of the electronic structure and adsorption showed that $CO_2$ is chemically adsorbed on Co-$C_3N_4$ and Fe-$C_3N_4$, but only weakly physisorbed on Ni-$C_3N_4$. The competitive hydrogen evolution reaction (HER) studies proved that all three of the systems are more selective to $CO_2$ reduction than HER. The reaction mechanism follows various initial protonation intermediates, with COOH preferred on Ni- $C_3N_4$ and OCHO on Co- and Fe- $C_3N_4$ and giving different $C_1$ product by different routes. Co- $C_3N_4$ was identified as the best catalyst

in the tested catalysts, with a more promising catalytic performance, as it was more active and selective to produce $CH_3OH$ because of lower limiting potential and a more desirable rate-limiting step [77].

**Ling Fu et al.** examined the electrocatalytic $CO_2$ reduction reaction (CRR) reaction in density functional theory (DFT) by embedding single metal atoms (Ti, V, Cr and Mn) into graphyne (GY) structures to attain high activity and selectivity at low overpotentials. Their research proves that the low overpotential with control of product selectivity is a major challenge in $CO_2$ conversion. Through reaction intermediates (COOH, CO and CHO) they can determine that Cr–GY was the best catalyst, as it is the one with the ultralow limiting potential of -0.29 V to produce $CH_4$. Competitive hydrogen evolution reaction (HER) experiment revealed that CO 2 binds exclusively to the active site on Cr-GY than that of $H_2$ and this is facilitated by higher $CO_2$ adsorption (-0.83 eV) than that of $H_2$ (-0.38 eV), thus inhibiting HER (limiting potential of HER -0.34 V). Overall, the present study indicates that Cr-embedded graphyne is a promising platform in the engineering of low-potential, high-activity, and selective electrocatalysts to reduce $CO_2$ [78].

**Yu Ren et al.** explored the electrochemical reaction of $CO_2$ reduction reaction ($CO_2RR$) on single-atom catalysts (SACs) on two-dimensional nanolayers of $MoS_2$ through density functional theory (DFT) in a systematic manner. A set of single atoms of the transition and noble metals (Fe, Co, Ni, Cu, Ru, Pd, and Pt) anchored on $MoS_2$ were tested and the results showed that the M@($MoS_2$) systems are highly selective to the reduction of $CO_2$, with most of the products being $CH_4$. Out of the known catalysts, the one that demonstrated the lowest limiting potentials of -0.39 V, -0.24 V, -0.45 V and -0.50 V were Fe@$MoS_2$, Co@$MoS_2$, Ni@$MoS_2$, and Pt@ $MoS_2$, respectively, giving them positive catalytic activity. The binding energy of the key intermediate, the HCOO, was found to be an efficient parameter used to screen good $CO_2RR$ catalysts. In addition, the paper showed that single-atom catalysts dispensed onto other chalcogenides, including $MoSe_2$, $WS_2$, and $WSe_2$, also possess a high potential of $CO_2$ reduction. Overall, the present work offers useful mechanistic information on SAC-driven $CO_2$ and demonstrates the designing capability of two-dimensional materials to create efficient and selective electrocatalysts [79].

**Neetu et al.** used the basis-set density functional theory (DFT) using numerical calculations to determine the mechanistic routes of the reduction of $CO_2$ to methanol on a long $CeO_2$ (110) surface. Their analysis analyzed thermochemistry of elementary reaction steps and identified the most preferable adsorption geometries and binding energies of the determining intermediates. A reaction pathway where carboxyl (COOH) and formate (HCOO) intermediates were formed was investigated. The findings demonstrated that the formate species is much more stable on stoichiometric ceria with a binding energy of -222.9 kJ mol -1, than the much weaker adsorption of the carboxyl intermediate (-36.0 kJ mol -1). Further hydrogenation of formate was however found to be highly endothermic to hydrogenate further to $H_2COOH$ after which the conversion to $H_2CO$ and OH was dissociative thus limiting the conversion of formate to methanol using this route. Conversely, the carboxyl-mediated pathway was generally exothermic on both stoichiometric and reduced ceria surfaces, except COOH dissociation step, which was moderately endothermic and had high activation barriers especially on stoichiometric ceria. Another direction of interest, which led to a lateral pathway to methane formation via CO intermediates, was the dissociation of CO which was found to be highly endothermic and as such, the formation of methane was unlikely. In general, this paper has indicated the importance of intermediate stability and activation barriers in ascertainment of the viability of $CO_2$ reduction mechanisms on ceria-based catalysts [80].

# 3 Computational Methodology

In the present work, all simulations were performed utilizing density functional theory as implemented in the Gaussian 16.B01 software package [81] and Gauss View 6.1.1 [82] will be used to visualize the results. B3LYP-D3/6-31+G (d,p) level of theory will be used to optimize the pristine and TMs doped $B_{12}N_{12}$ SAC structure at the DFT (Density Functional Theory) level. At the same theoretical level, vibrational frequency will be calculated to identify the stationary point on the potential energy surface (PES). B3LYP is a hybrid DFT functional recognized for its efficacy in performing quantum chemical calculations to identify the electronic characteristics and thermodynamic stability of chemical compounds [83]. Moreover, B3LYP has been extensively employed for the optimization and mechanistic analysis of nanocages [84][85]. Grimme's dispersion (D3) was utilized in our computations to examine the dispersion correction[86]. The stabilities of complexes (metal doped on $\mathbf{B_{12}N_{12}}$) will be investigated using the interaction energies of optimized geometries. The following equation will be used to calculate the interaction energy ($E_{ads}$)

$$\mathbf{E_{int}} = \mathbf{E_{TM@B12N12}} - (\mathbf{E_{B12N12}} + \mathbf{E_{TM}}) \qquad \textbf{(1)}$$

In this equation, $\boldsymbol{E_{TM@B12N12}}$ represents the energy of transition metal doped $B_{12}N_{12}$ nanocage, $\boldsymbol{E_{TM}}$ represents energy of isolated transition metal and $\boldsymbol{E_{B12N12}}$ represents energy of $B_{12}N_{12}$ nanocage [65]. Then $H_2$ and $CO_2$ were adsorbed on TM doped SAC and to calculate the adsorption energy of $CO_2$ and $H_2$ molecules on surface of $B_{12}N_{12}$, following equation will be used.

$$\mathbf{E_{ads}} = \mathbf{E_{adsorbate@TM@B12N12}} - (\mathbf{E_{TM@B12N12}} + \mathbf{E_{CO2}}) \qquad \textbf{(2)}$$

$\mathbf{E_{adsorbate@TM@B12N12}}$ represent the energy of adsorbed molecule on the surface of metal doped $\mathbf{B_{12}N_{12}}$, $\mathbf{E_{TM\text{-}B12N12}}$ is the energy of complex of metal embedded $\mathbf{B_{12}N_{12}}$ surface and $\mathbf{E_{CO2}}$ accounts for the energy of $CO_2$ molecule [87].

To investigate perturbation in electronic level, frontier molecular orbitals (FMOs) analysis has been carried out for TM@$B_{12}N_{12}$ complexes. HOMO-LUMO energies were determined and $G_{HL}$ was obtained and compared with pristine $B_{12}N_{12}$. NBO has been performed at same level of theory to confirm the charge transfer and reactivity of TM@$B_{12}N_{12}$ complexes. QTAIM and IRI analysis has been performed to study the types of interactions among transition metal atom

and $B_{12}N_{12}$ nanocage. Different parameters like Laplacian ($\boldsymbol{\nabla^2 \rho}$), energy density of all electrons ($\boldsymbol{\rho}$) and H(r) were considered for determining the type of interaction between TM and $B_{12}N_{12}$. The results of these analyses are obtained with Multiwfn [88] and VMD [89] software. Molecular electrostatic potential (MEP) analysis has been carried out to locate the electrophilic and nucleophilic region on both pristine $B_{12}N_{12}$ and TM@$B_{12}N_{12}$ complexes.

Following equations will be used to determine the energy barrier ($E_a$) and the energy of reaction ($\Delta E$), in the respective way,

$$\mathbf{E_a = E_{TS} - E_R} \quad \textbf{(3)}$$

$$\mathbf{\Delta E = E_P - E_R} \quad \textbf{(4)}$$

In $CO_2$ reduction reaction, $E_{TS}$ stands for transition state energy, $E_R$ for reactant energy, and $E_P$ for product energy. The activation energy, or $E_a$, is the energy threshold that reactants must cross to start the reaction of $CO_2$ reduction.

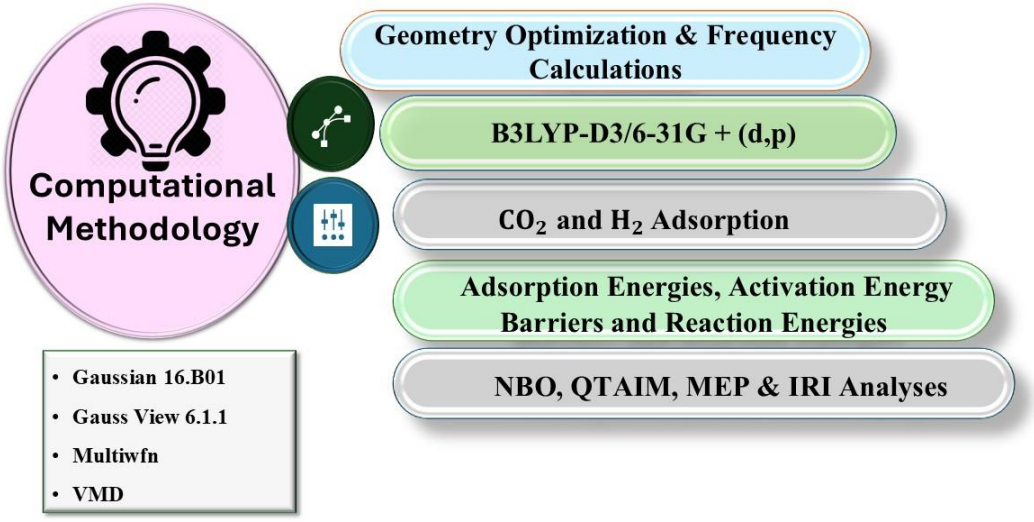


Figure 3.1 Computational Methodology

# 4 Results and Discussions

## 4.1 Geometry Optimization

Geometry optimization of transition-metal (TM) doped $B_{12}N_{12}$ nanocages was carried out using density functional theory (DFT) at the B3LYP-D3/6-31G+(d,p) level of theory, which incorporates Grimme's dispersion correction to properly account for long-range interactions. Pristine $B_{12}N_{12}$ includes eight six-membered and six four- membered rings. In this structure, the B-N bond length is estimated to be 1.44 Å in six-membered rings and 1.48 Å in four-membered rings. To systematically examine the effect of dopant position on structural stability, the TM atom was introduced at six distinct adsorption or substitutional sites of the nanocage, namely **b64 and b66**, corresponding to B–N bond bridge sites shared by four- and six-membered rings; **r4 and r6**, located at the centers of four- and six-membered rings, respectively; and **Btop and Ntop**, where the dopant is placed directly above a boron or nitrogen atom on the cage surface. These positions offer different coordination environments and electronic surroundings for the dopant atom. Upon optimization, TM incorporation induces localized structural distortions around the adsorption site while largely preserving the overall cage framework, indicating that the stability and geometric response of the $B_{12}N_{12}$ nanocage are strongly dependent on the specific doping position [90].

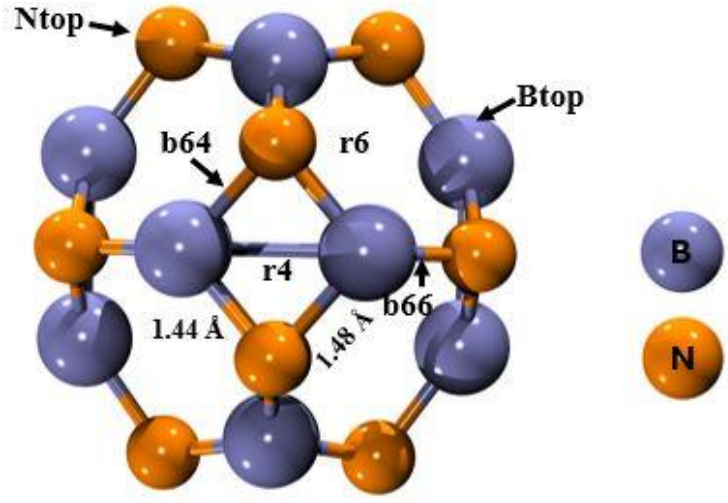


Figure 4. 3 Optimized Geometry of $B_{12}N_{12}$

Energies of all possible positions are shown in Table 4.1.

| Metal | b64 | b66 | Btop | Ntop | r4 | r6 |
|---|---|---|---|---|---|---|
| **Fe** | **-2219.6496** | -2219.5975 | -2219.5975 | -2219.5975 | -2219.6496 | -2219.6492 |
| **Co** | **-2338.7153** | -2338.7142 | -2338.7142 | -2338.7142 | -2338.7153 | -2338.7155 |
| **Ni** | **-2464.2496** | -2464.2324 | -2464.2324 | -2464.2324 | -2464.2496 | -2464.2491 |
| **Cu** | **-2596.3945** | -2596.3427 | -2596.3427 | -2596.3926 | -2596.3945 | -2596.3943 |
| **Zn** | **-2735.2579** | -2735.2579 | -2735.2579 | -2735.2579 | -2735.2579 | -2735.2416 |

Table 4. 2 Energies on possible positions

After analyzing the energies on all these positions, it was found that b64 is the most stable site for TM doping as the doped metal is surrounded by equivalent number of boron and nitrogen atoms at comparable distances due to which there is reduced strain which further leads to enhanced orbital overlap and efficient charge transfer. The optimized geometries of TM doped $B_{12}N_{12}$ are given in figure 4.2.

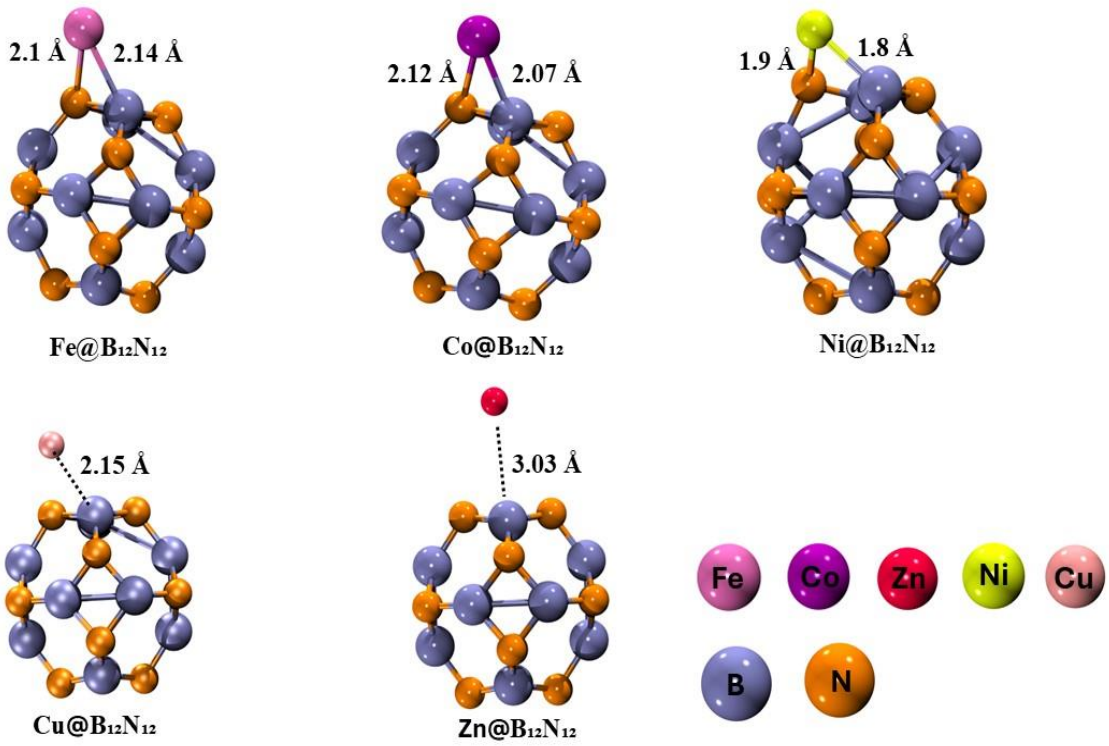


Figure 4. 4 Optimized Geometries of TM doped $B_{12}N_{12}$

## 4.2 Energetic Analysis and Thermodynamic Stability

By calculating the interaction energy of each TM doped complex (Fe-Zn), thermodynamic stability of complex was assessed. Interaction energies of each TM doped complex is shown in Table 4.2.

| **M@$B_{12}N_{12}$** | Hartree | eV |
|---|---|---|
| **Fe@$B_{12}N_{12}$** | **-0.1549** | **-4.21** |
| **Co@$B_{12}N_{12}$** | -0.0401 | -1.09 |

| | | |
|---|---|---|
| **Ni@$B_{12}N_{12}$** | -0.0896 | -2.43 |
| **Cu@$B_{12}N_{12}$** | -0.0146 | -0.39 |
| **Zn@$B_{12}N_{12}$** | -0.0062 | -0.16 |

Table 4.2 Interaction energies (eV) of TM doped $B_{12}N_{12}$

The thermodynamic stability of all these complexes is indicated by the negative values of interaction energy for all TMs@$B_{12}N_{12}$. Interaction values range from -4.21 eV for Fe@$B_{12}N_{12}$ to -0.16eV for Zn@$B_{12}N_{12}$ which confirms the chemisorption of Fe, Co and Ni doped complexes and physisorption of Cu and Zn doped complexes. A monotonic trend is observed in the interaction energy values, with Fe@$B_{12}N_{12}$ exhibiting the highest interaction energy owing to the partially filled $d^6$ electronic configuration of Fe, which provides readily accessible d orbitals for effective bonding. This facilitates strong charge transfer from Fe to the electron-deficient boron atoms along with back-donation from nitrogen, resulting in a strong metal–cage interaction. As the series progresses to Co ($d^7$), the increased filling of the d orbitals reduces their availability for bonding, leading to a decrease in interaction energy. In the case of Ni, a slight increase in interaction strength is observed, which can be attributed to its singlet spin state that induces a more directional electron density, thereby enhancing metal–nitrogen σ-donation. In contrast, Cu and Zn, with nearly filled and fully filled d orbitals ($d^{10}$), respectively, exhibit limited orbital participation in bonding with the $B_{12}N_{12}$ cage. As a result, their interaction is dominated by weak van der Waals forces, corresponding to physisorption and the lowest interaction energy values among the studied systems.

## 4.3 Charge Analysis

The amount of charge transfer between metal atom and $B_{12}N_{12}$ was determined by natural bond order (NBO) analysis. As it is known that metals are electropositive in nature due to which transition metal should transfer extra electrons to $B_{12}N_{12}$ cage. NBO analysis confirmed that net positive charge is present on metal atom which means that extra electrons are transferred

from transition metal to $B_{12}N_{12}$ cage. The amount of charge transfer in complexes Fe@$B_{12}N_{12}$, Co@ $B_{12}N_{12}$, Ni@ $B_{12}N_{12}$, Cu@ $B_{12}N_{12}$ and Zn@ $B_{12}N_{12}$ is 0.520, 0.469, 0.485, 0.334 and 0.016 |e| respectively is shown in **Table 4.3**. The charge transfer decreases in the order **Fe > Ni > Co > Cu > Zn**, where Fe shows the highest electron donation due to its partially filled d orbitals. As the d orbitals become progressively filled from Co to Ni, the availability of electrons for donation decreases, leading to reduced charge transfer. In Cu, the nearly filled d shell further restricts electron donation, while Zn, with a fully filled $d^{10}$ configuration, exhibits minimal charge transfer, indicating weak metal–cage interaction.

| **TM@$B_{12}N_{12}$** | **Q \|e\|** | **$E_{HOMO}$ (eV)** | **$E_{LUMO}$ (eV)** | **$G_{HL}$ (eV)** |
|---|---|---|---|---|
| **$B_{12}N_{12}$** | - | -7.95 | -1.23 | 6.72 |
| **Fe@$B_{12}N_{12}$** | 0.520 | -5.21 | -2.25 | 2.96 |
| **Co@$B_{12}N_{12}$** | 0.469 | -5.24 | -2.12 | 3.12 |
| **Ni@$B_{12}N_{12}$** | 0.485 | -6.23 | -2.88 | 3.35 |
| **Cu@$B_{12}N_{12}$** | 0.334 | -5.18 | -2.02 | 3.16 |
| **Zn@$B_{12}N_{12}$** | 0.016 | -6.64 | -1.64 | 5.00 |

Table 4.3 The NBO charges Q (|e|), EHOMO (eV), ELUMO (eV), Energy gaps $G_{HL}$

## 4.4 Frontier Molecular Orbital (FMO) Analysis

Frontier Molecular Orbital (FMO) analysis is used to determine highest occupied molecular orbitals (HOMOs) and lowest unoccupied molecular orbitals (LUMOs) energies and iso-

densities. HUMO and LUMO energy gap difference, which is also known as $G_{HL}$ gives us information about microelectronic properties of complexes such as conductance, semi-conductance and insulation properties [91]. The homo-lumo gap in pristine $B_{12}N_{12}$ nanocage is 6.72 eV which is comparable with the previous results [90]. It is depicted in the results shown in Table 4.3 that homo-lumo gap in TM doped complexes is far less compared to pristine $B_{12}N_{12}$ nanocage. This reduction mainly originates from charge transfer from the transition metal to the $B_{12}N_{12}$ cage, which introduces new electronic states near the Fermi level. Consequently, a new HOMO level is formed while the original HOMO shifts to a lower energy level (HOMO–1), leading to a narrowed band gap. Among the studied systems, $Fe@B_{12}N_{12}$ exhibits the smallest HOMO–LUMO gap, which can be attributed to its higher charge transfer and partially filled d orbitals that strongly interact with the cage framework. In contrast, $Zn@B_{12}N_{12}$ shows a larger gap due to minimal charge transfer arising from its fully filled $d^{10}$ configuration. Overall, the reduced GHL values for all TM-doped complexes compared to pristine $B_{12}N_{12}$ demonstrate enhanced electronic activity and reactivity of the doped nanocages. This trend of homo-lumo gap is comparable with the previous study done by Maryam et al, on transition metal doped on $B_{12}N_{12}$ nanocage [92]. The graphical representation of HOMOs and LUMOs is shown in **figure 4.3.** It is demonstrated that electron densities of HOMOs are located on transition metal as it leads to formation of new HOMOs level and LUMOs electron densities are located on $B_{12}N_{12}$ nanocage.

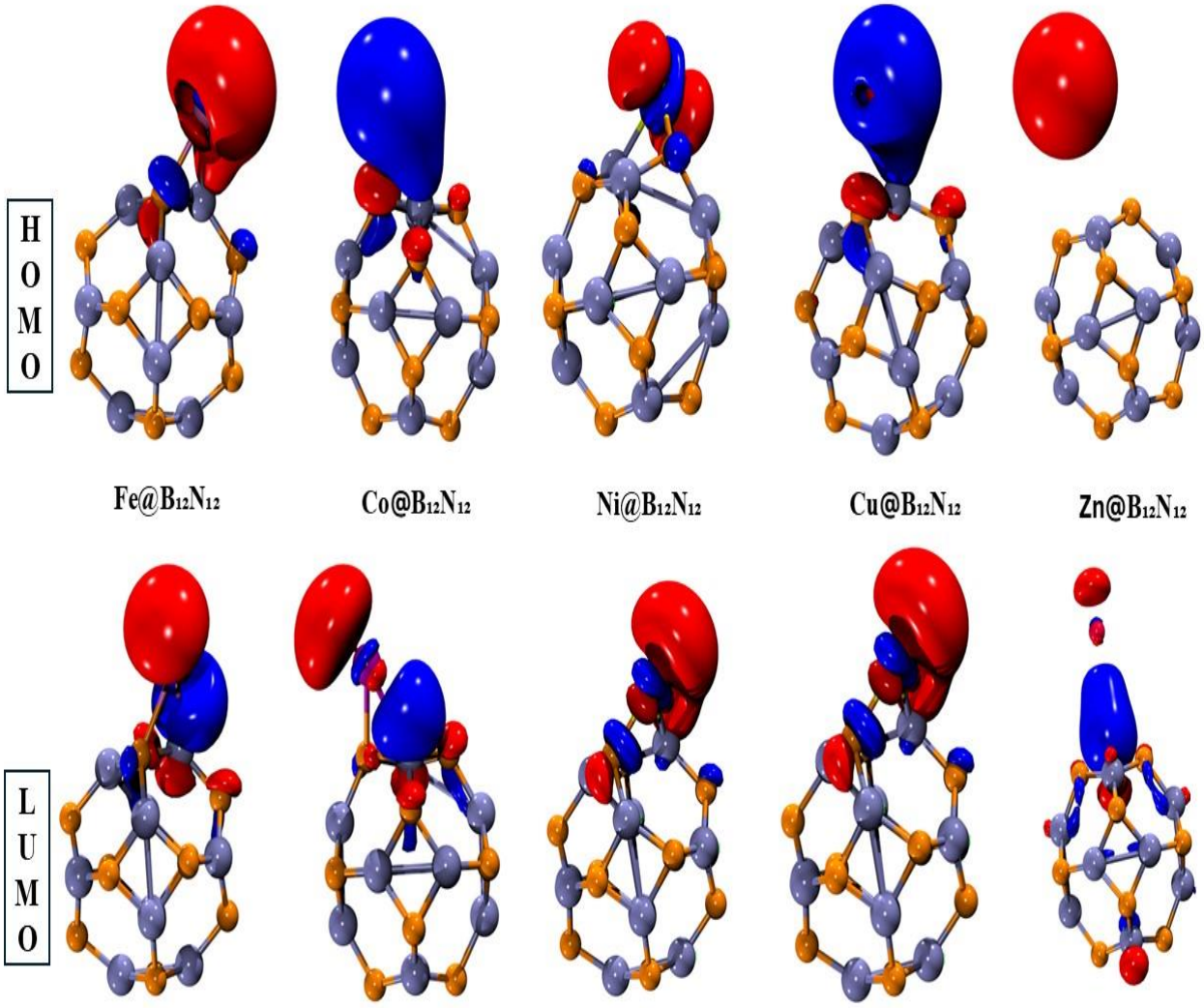


4.3 Frontier Molecular Orbital Diagram of all complexes

## 4.5 Molecular Electrostatic Potential

MEP analysis is used to represent the distribution of electronic charge and thus it is valuable tool for identifying electrophilic and nucleophilic regions of complex that can further help in predicting $H_2$ and $CO_2$ interactions [93]. MEP surface of TM doped complexes (Fe-Zn) is shown in Figure **4.4.** Color gradient was applied to visualize the electrostatic potential distribution across the surface. Zero, negative and positive potential was represented by white, red and blue regions. From MEP of TM doped complexes, it is evident that blue region is present around transition metal which indicates that electron deficient region is created due to transfer of electron from TM to $B_{12}N_{12}$ nanocage. In case of Fe, Co and Ni doped complexes,

prominent blue region is present on TM as there is efficient charge transfer between TM and cage but in case of Cu and Zn doped complex, no definite blue region can be identified which means poor charge transfer which is also consistent with NBO and interaction energy calculations.

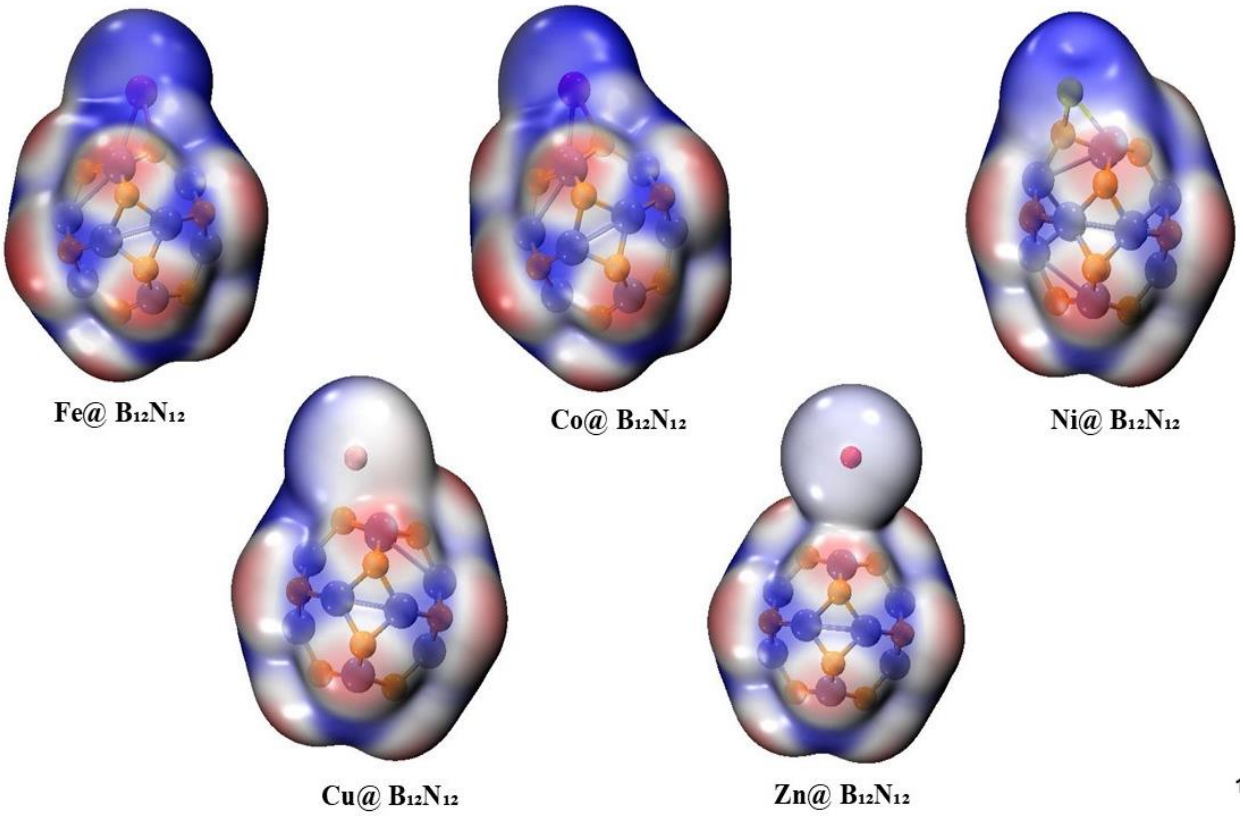


Figure 4.4 MEP Diagram of TM doped $B_{12}N_{12}$ complexes

## 4.6 Quantum Theory of Atoms in Molecules (QTAIM) Analysis

When transition metals are doped on $B_{12}N_{12}$ cage, different kinds of interactions occur. In order to examine the nature of interactions, QTAIM analysis is performed [94]. Different topological parameters like electron density(ρ), Laplacian electron density ($\nabla^2 \rho$) and electronic energy density (H)(r) are employed to determine the nature of bond [95]. These parameters at different BCPs are listed in **Table 4.4.**

| **TM@$B_{12}N_{12}$** | **BCPs** | **ρ** | **$\nabla^2 \rho$** | **H r** | **V r** | **G r** | **-G r/V r** |
|---|---|---|---|---|---|---|---|
| **Fe@$B_{12}N_{12}$** | Fe-B | 0.0741 | -0.0198 | -0.0374 | -0.0698 | 0.0324 | 0.464 |
| | Fe-N | 0.0720 | 0.2681 | -0.0137 | -0.0945 | 0.0808 | 0.855 |
| **Co@$B_{12}N_{12}$** | Co-B | 0.0834 | 0.0554 | -0.0473 | -0.0807 | 0.0334 | 0.413 |
| | Co-N | 0.0652 | 0.2746 | -0.0143 | -0.0973 | 0.0830 | 0.853 |
| **Ni@$B_{12}N_{12}$** | Ni-B | 0.125 | -0.182 | -0.0939 | -0.142 | 0.0482 | 0.339 |
| | Ni-N | 0.143 | 0.511 | -0.0575 | -0.242 | 0.185 | 0.764 |
| **Cu@$B_{12}N_{12}$** | Cu-B | 0.0630 | 0.0417 | -0.0239 | -0.0582 | 0.0343 | 0.589 |
| **Zn@$B_{12}N_{12}$** | Zn-B | 0.0038 | 0.0071 | 0.0003 | -0.0011 | 0.0014 | 1.272 |

Table 4.4 Topological Analysis of Transition metal doped $B_{12}N_{12}$ complexes

According to Bader's theory, the nature of interaction between a dopant and a substrate can be classified using topological parameters of electron density. Covalent interactions are indicated when $\nabla^2\rho < 0.0$, $H(r) < 0.0$, and $-G(r)/V(r) < 1.0$, with stronger covalent character observed for $\rho(r) > 0.1$ and $-G(r)/V(r) < 0.5$. Partial covalent interactions are identified when $\nabla^2\rho > 0.0$ and $H(r) < 0.0$, whereas non-covalent interactions are characterized by $\nabla^2\rho > 0.0$, $H(r) > 0.0$, and $-G(r)/V(r) > 1.0$ [96]. The topological diagram of all the transition metal doped complexes is shown in **Figure 4.5.** Fe, Co and Ni doped complexes have one partial covalent and one covalent bond while copper has only one partial covalent bond with boron and only Zn doped complex has one non-covalent bond with boron.

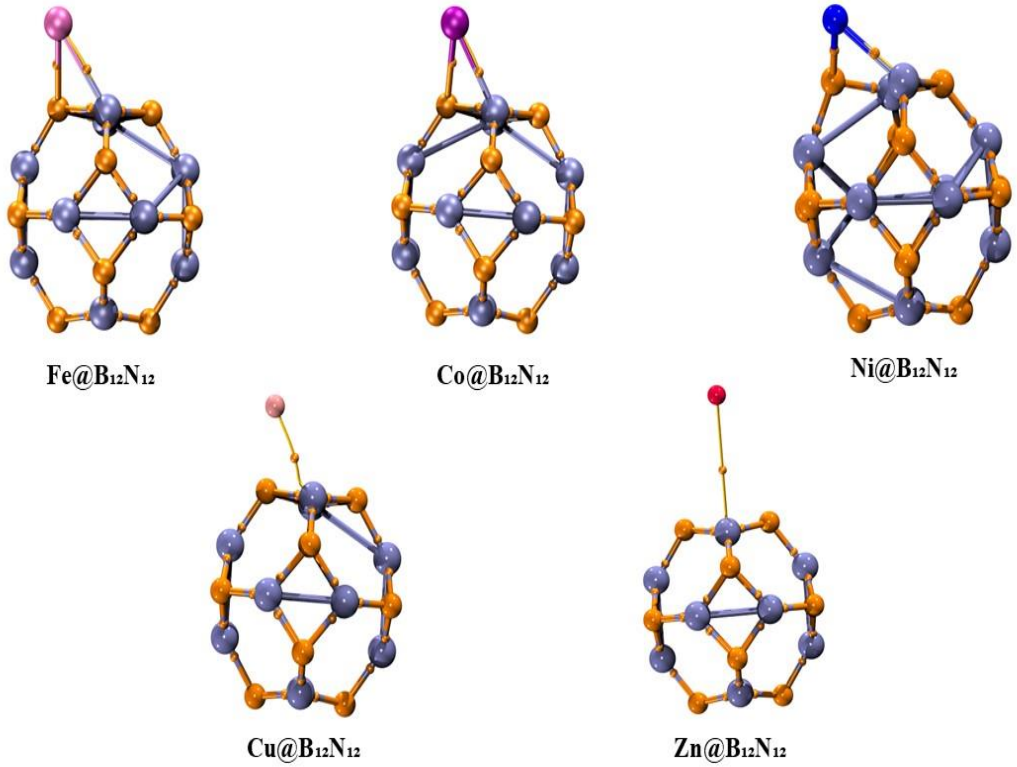


Figure 4.5 QTAIM Analysis of TM doped $B_{12}N_{12}$ complexes

## 4.7 Hydrogen Adsorption on TM doped complexes

As discussed in the preceding results, the charge transfer between the metal atom and the nanocage is minimal in the case of Cu and Zn-doped complexes, resulting in the absence of pronounced blue regions in their molecular electrostatic potential (MEP) maps. This indicates the lack of a significant electrophilic region at the metal center, which is a key requirement for effective $H_2$ adsorption. Consequently, these two complexes were excluded from further adsorption studies. Hydrogen molecules were subsequently adsorbed on Fe, Co, and Ni-doped complexes, with an initial H–H bond length of 0.74 Å and the optimized geometries are shown in **Figure 4.6.** The corresponding adsorption energies were calculated and are reported in **Table 4.5.** Notably, in the cases of Ni and Co-doped complexes, relatively higher adsorption energies were observed, accompanied by an elongation of the H–H bond to 0.83 Å and 0.75 Å,

respectively. This bond elongation signifies the effective activation of $H_2$ on these metal-doped nanocages.

| $H_2M@B_{12}N_{12}$ | Initial H-H distance | Activated H-H distance | Adsorption Energy (eV) |
|---|---|---|---|
| $H_2Co@B_{12}N_{12}$ | 0.74 Å | 0.75 Å | -0.09 |
| $H_2Ni@B_{12}N_{12}$ | 0.74 Å | 0.83 Å | -1.10 |
| $H_2Fe@B_{12}N_{12}$ | 0.74 Å | 0.74 Å | -0.07 |

Table 4.5 Adsorption energies of $H_2$ on TM doped complexes

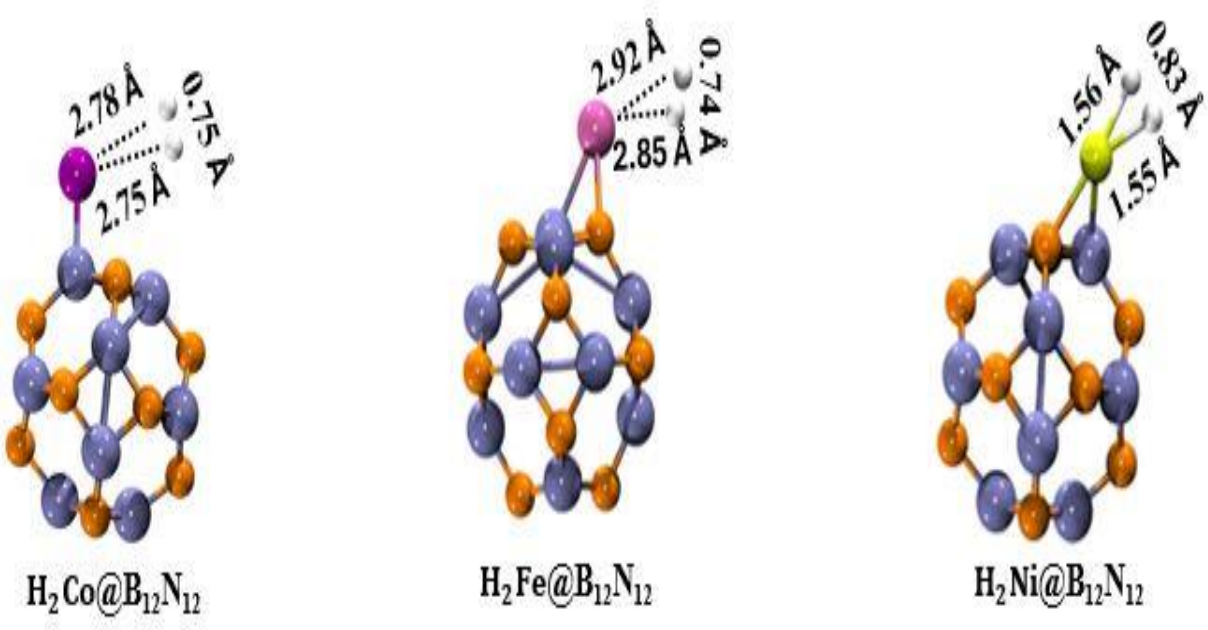


Figure 4.6 Optimized Geometries of $H_2$ adsorbed complexes

## 4.8 $CO_2$ adsorption on TM doped complexes

The optimized geometries of $CO_2$ adsorbed on Fe, Co, and Ni-doped $B_{12}N_{12}$ complexes shown in **figure 4.7** demonstrate clear variations in adsorption strength and activation behavior. Upon adsorption, the initially linear $CO_2$ molecule undergoes a noticeable bending deformation, signifying activation through charge transfer from the metal centers to the antibonding orbitals of $CO_2$, which weakens the C–O bonds. Molecular parameters related to $CO_2$ molecule on TM doped complex and adsorption energy of $CO_2$ are shown in **Table 4.6.**

| **$CO_2M@B_{12}N_{12}$** | O=C=O Angle | C=O distance | Adsorption Energy (eV) |
|---|---|---|---|
| **$CO_2Fe@B_{12}N_{12}$** | 135.7 | 1.19 Å | -0.13 |
| **$CO_2Co@B_{12}N_{12}$** | 126.1 | 1.32 Å | -1.01 |
| **$CO_2Ni@B_{12}N_{12}$** | 150.1 | 1.18 Å | -1.14 |

Table 4.6 Molecular Parameters and Adsorption Energy of $CO_2$ on TM doped complexes

Among the studied systems, $Ni@B_{12}N_{12}$ exhibits the highest $CO_2$ adsorption energy (−1.14 eV), which can be attributed to the optimal overlap between Ni d orbitals and $CO_2$ $\pi^*$ orbitals, along with sufficient charge transfer that strongly stabilizes the adsorbed molecule. In contrast, $Fe@B_{12}N_{12}$ shows the weakest adsorption (−0.14 eV) due to comparatively lower charge redistribution toward $CO_2$ and less effective orbital interaction, resulting in a weaker binding nature. Notably, $Co@B_{12}N_{12}$ presents a particularly favorable adsorption geometry, where $CO_2$ adopts a metal–$CO_2$–cage bridging configuration in which the carbon atom binds to the cobalt center while one oxygen atom simultaneously interacts with the cage. This dual-interaction mode enhances charge redistribution, induces pronounced $CO_2$ bending, and leads to effective activation of the C–O bonds. Although the adsorption energy of $Co@B_{12}N_{12}$ is slightly lower than that of $Ni@B_{12}N_{12}$, the cooperative metal– and cage–adsorbate interactions render cobalt-

doped $B_{12}N_{12}$ geometrically and electronically more favorable than the iron-doped system, highlighting its potential for efficient $CO_2$ activation.

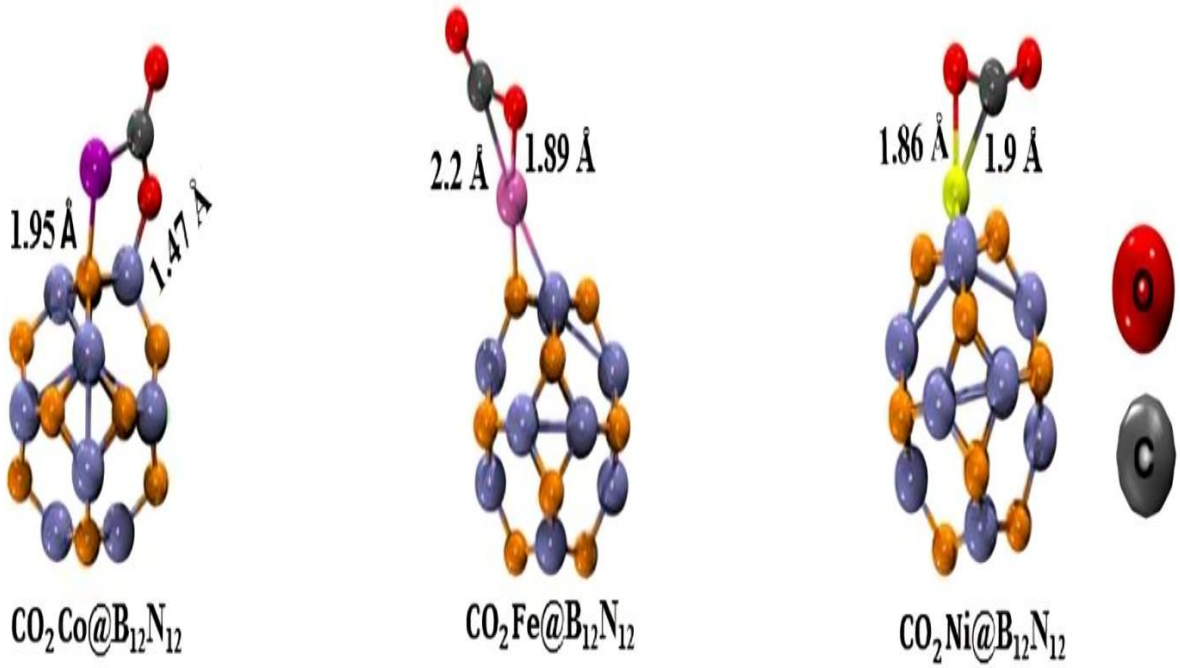


Figure 4.7 Optimized geometries of $CO_2$ adsorbed on TM doped complexes

## 4.9 Co-adsorption of $H_2$ and $CO_2$

As discussed previously, adsorption energy of $CO_2$ is greater than that of $H_2$ so the catalytic hydrogenation of $CO_2$ will be initiated with $CO_2$ adsorption on TM doped complex. After the initial adsorption of $CO_2$ on the TM-doped $B_{12}N_{12}$ nanocages, the interaction of $H_2$ with the pre-adsorbed $CO_2$ systems was investigated to evaluate the activation capability of the catalyst. As shown in **figure 4.8**, a clear distinction is observed among the optimized geometries of Fe, Co, and Ni-doped complexes. In the cases of $Fe@B_{12}N_{12}$ and $Ni@B_{12}N_{12}$, the $H_2$ molecule remains almost intact with an H–H bond length close to its gas-phase value (~0.74 Å), indicating molecular adsorption without activation. This behavior can be attributed to the relatively weak interaction between $H_2$ and the metal centers after $CO_2$ adsorption, as the metal d orbitals are either insufficiently available or already engaged in stabilizing the $CO_2$ molecule, thereby limiting effective back-donation into the σ* orbital of $H_2$. In contrast, the Co-doped complex exhibits pronounced $H_2$ activation, as evidenced by the noticeable elongation of the

H–H bond (~0.78–0.79 Å). This activation arises from the favorable electronic environment of cobalt, which enables simultaneous interaction with both $CO_2$ and $H_2$ through its partially filled d orbitals. The presence of a metal–$CO_2$–cage bridging configuration in $Co@B_{12}N_{12}$ facilitates enhanced charge redistribution, allowing efficient σ-donation from $H_2$ to Co and π-back-donation from Co to the antibonding orbital of $H_2$. Consequently, only the cobalt-doped system demonstrates effective $H_2$ activation following $CO_2$ adsorption, highlighting its superior catalytic potential compared to the Fe and Ni doped counterparts.

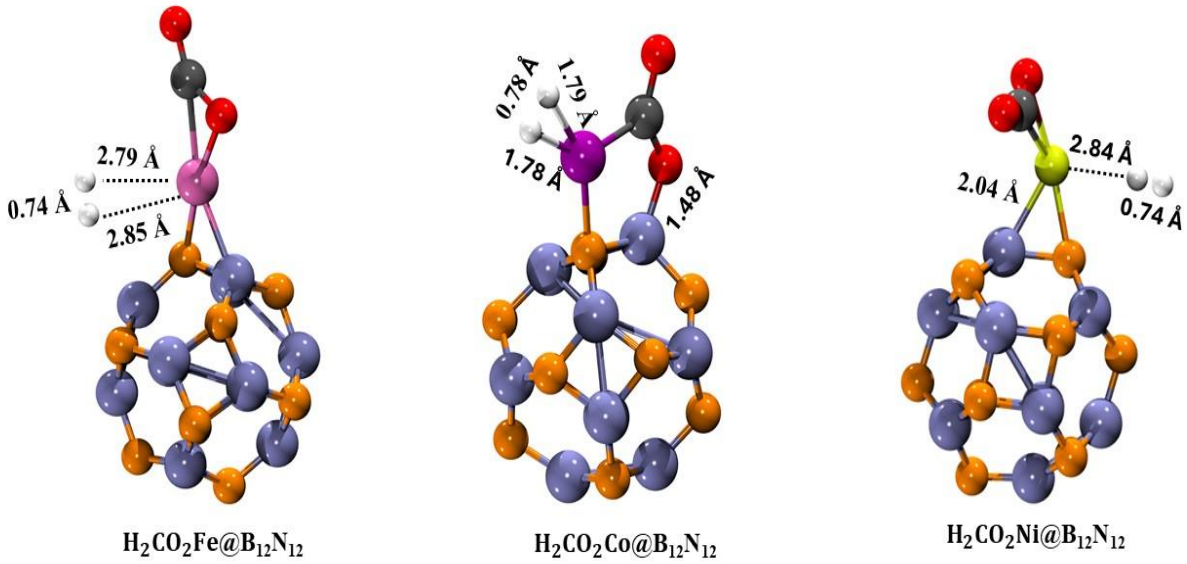


Figure 4.8 Optimized geometries of $H_2$ and $CO_2$ co-adsorption

## 4.10 IRI Analysis of $H_2$ and $CO_2$ co-adsorbed Complexes

In 2021, Lu et al. introduced the Interaction Region Indicator (IRI) method as an advancement over the widely used RDG approach, addressing its limitation in accurately describing covalent interactions [97]. IRI analysis is valuable for studying chemical reactions as it can effectively reveal the smooth transitions between weak interactions and chemical bonds [98]. Three colors

are depicted in 3D isosurfaces and 2D IRI graphs. Blue represents covalent interactions; green represents weak van der Waal interactions and red represents steric repulsions. 3D isosurfaces and 2D IRI graphs are shown in **figure 4.9.** IRI analysis revealed that Co@$B_{12}N_{12}$ complex have covalent interactions (blue patch) for both $CO_2$ and $H_2$ while Ni@$B_{12}N_{12}$ and Fe@$B_{12}N_{12}$ complexes both have covalent interaction for $CO_2$ but weak van der Waal interactions (green patch) for $H_2$ which means that these two complexes only activated $CO_2$.

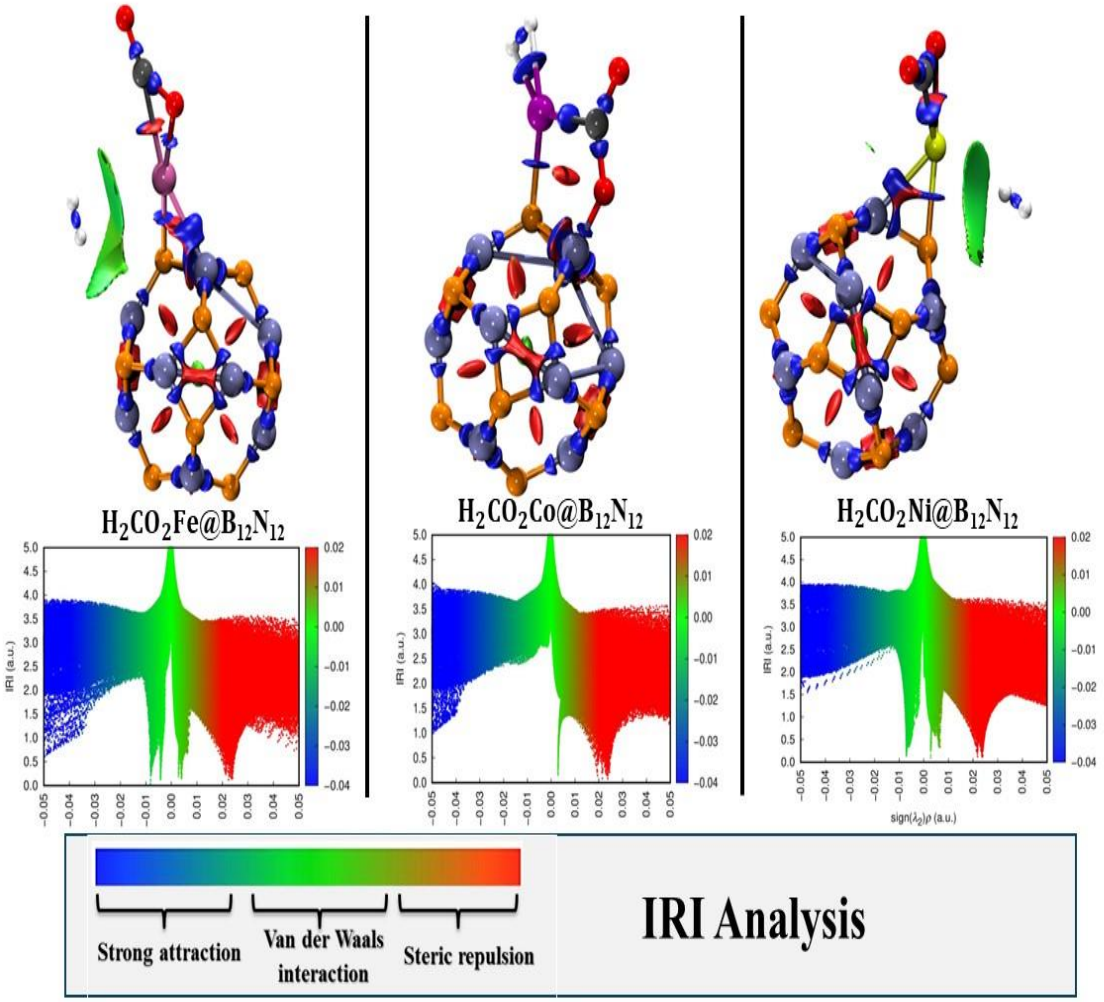


Figure 4.9 IRI Analysis of $H_2$ and $CO_2$ adsorbed Complexes

## 4.11 $CO_2$ Reduction to Formic Acid over TM@$B_{12}N_{12}$ Catalyst

The reduction of $CO_2$ to formic acid on TM-doped $B_{12}N_{12}$ nanocages proceeds via a Langmuir–Hinshelwood (LH) mechanism, which is consistent with the work presented by Abedini et al.

[99]. In this mechanism, both reactants $CO_2$ and $H_2$ are initially adsorbed on the catalyst surface prior to reaction. Molecular hydrogen undergoes dissociative adsorption on the active metal site, generating surface-bound hydrogen species (H*), while $CO_2$ is activated through metal–adsorbate interactions. The subsequent hydrogenation occurs through stepwise proton–electron transfer involving adsorbed intermediates, leading to the formation of Formate or Carboxyl and then leading to formation of formic acid. This surface-mediated pathway enables effective charge redistribution and bond activation, particularly evident in cobalt-doped systems where strong metal–adsorbate coupling stabilizes key intermediates.

As summarized in **Table 4.6**, the $Co@B_{12}N_{12}$ complex exhibits superior performance compared to other metal-doped systems in terms of $CO_2$ activation, as evidenced by the significant elongation of the C=O bond to 1.32 Å, which reflects bond weakening and effective molecular activation conducive to subsequent chemical transformation. Furthermore, **Figure 4.9** clearly demonstrates that $Co@B_{12}N_{12}$ is the only doped complex capable of activating molecular hydrogen, as indicated by the increase in the H–H bond length from 0.74 Å to 0.78 Å upon adsorption. This simultaneous activation of both $CO_2$ and $H_2$ highlights the unique catalytic capability of the cobalt-doped nanocage. Consequently, $CO_2$ reduction reactions were systematically investigated on the $Co@B_{12}N_{12}$ complex via two mechanistic routes, namely the Formate and Carboxyl pathways, to elucidate the preferred reaction mechanism and associated energy profiles.

## 4.12 Mechanisms of $CO_2$ reduction on $Co@B_{12}N_{12}$

CO2 hydrogenation to formic acid can occur via two pathways. In this mechanism, $CO_2$ and $H_2$ are adsorbed on Cobalt doped complex. In the next step, Intermediate is formed in which Hydrogen molecule is activated and H-H distance increases up to 0.78 Å. After the formation of first intermediate IS1, mechanism is divided into two possible paths, **Formate (Path A) and Carboxyl (Path B)**. In path A, first transition state TS1 is formed in which H-H distance increases up to 0.94 Å and one hydrogen atom approaches carbon of $CO_2$. After passing through TS1, next intermediate is formed in which one hydrogen is attached to carbon atom of $CO_2$ and formate is formed on surface. In second transition state TS2, the second hydrogen

atom approaches oxygen atom and after passing through TS2, formic acid is formed on surface. Detailed schematic diagram of formate pathway is shown in **Figure 4.10.**

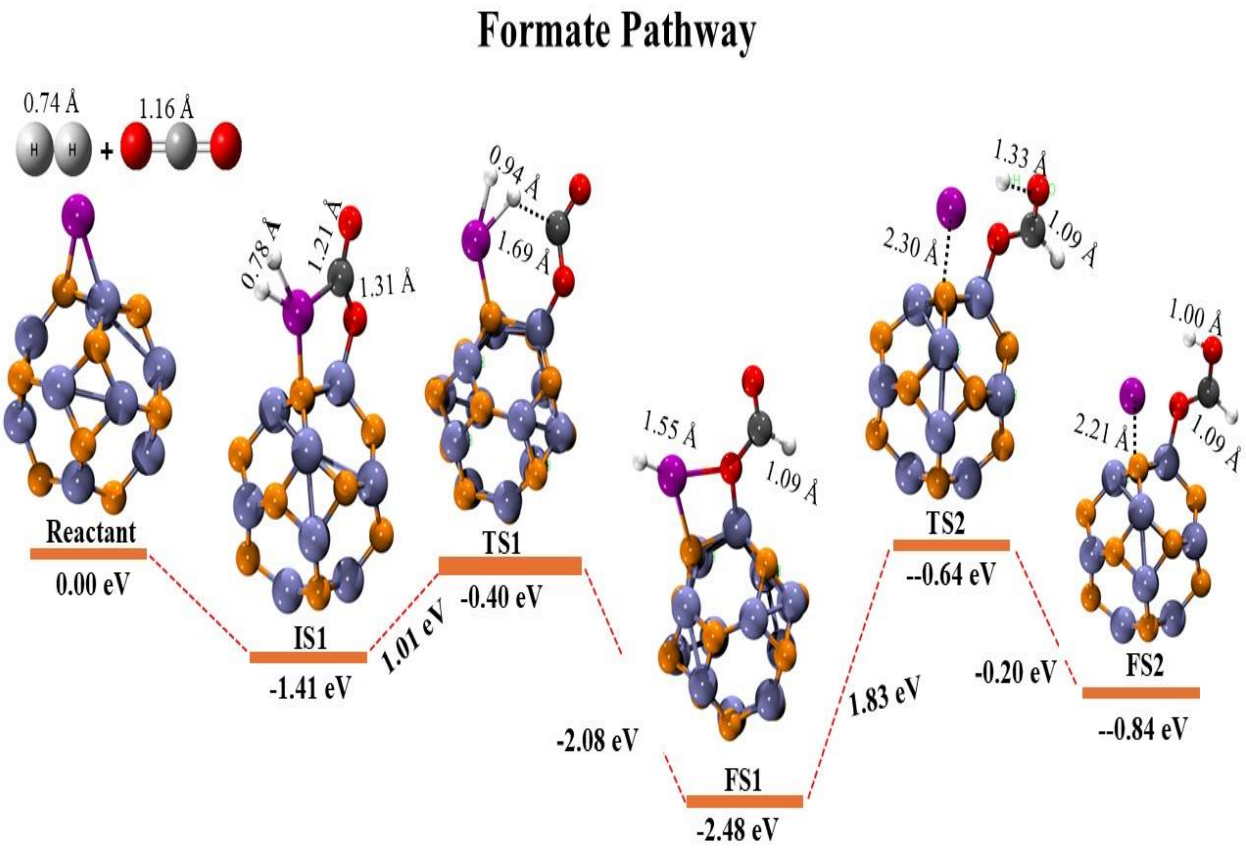


Figure 4.10 Schematic Diagram of Formate pathway

In path B, first transition state TS1 is formed in which H-H distance increases up to 1.01 Å and this time first hydrogen approaches oxygen atom of $CO_2$. After passing through TS1, carboxyl is formed on surface. After passing through TS2, another hydrogen atom attaches to carbon atom leading to formation of formic acid. Detailed schematic diagram of Carboxyl pathway is shown in **Figure 4.11.**

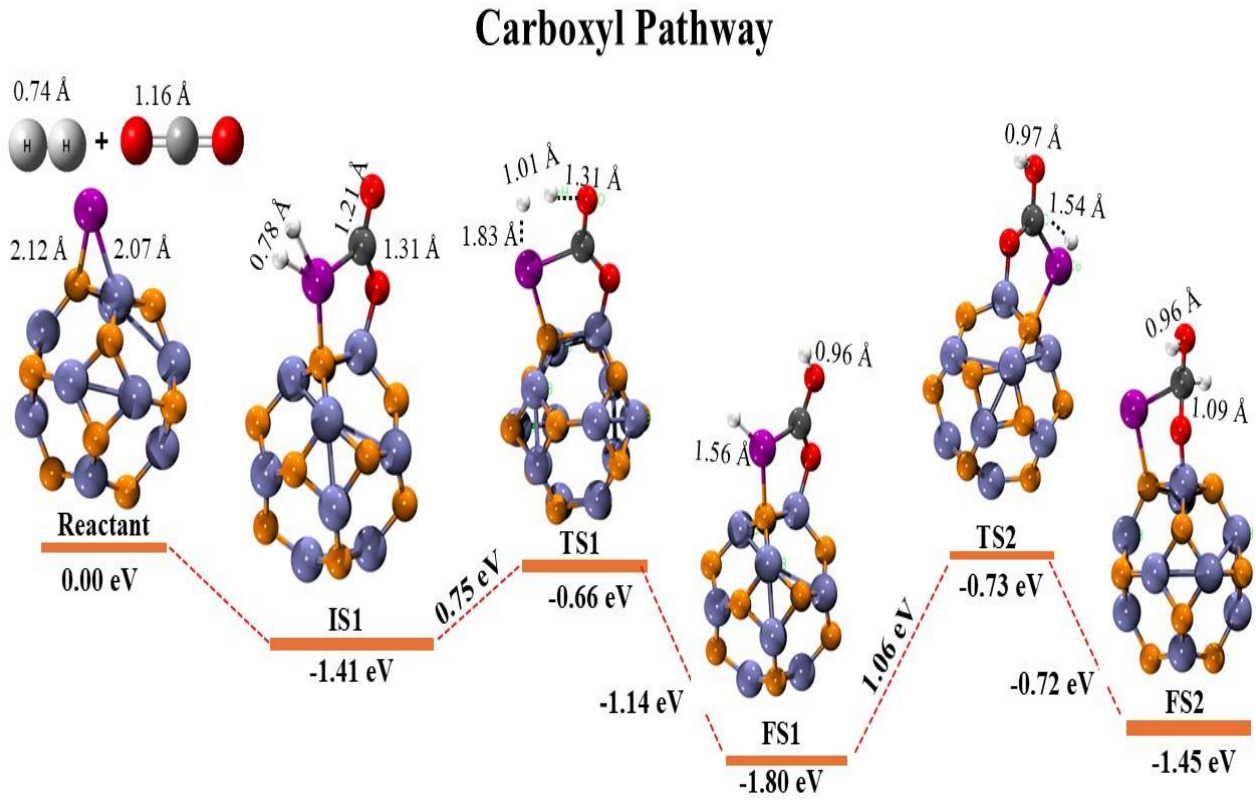


Figure 4.11 Schematic Diagram of Carboxyl Pathway

## 4.13 Comparison of Energy Profiles of Pathways

A detailed comparison of the **formate (Path A)** and **carboxyl (Path B)** pathways for $CO_2$ reduction to formic acid on the $Co@B_{12}N_{12}$ catalyst reveals clear differences in both kinetic and thermodynamic aspects. From a kinetic perspective, the rate-determining step **(RDS)** in the formate pathway corresponds to the **FS1 → TS2** step, which exhibits a relatively high activation barrier of **1.83 eV**, indicating a kinetically demanding hydrogen transfer process. In contrast, the carboxyl pathway shows a significantly lower activation barrier for its **RDS (FS1 → TS2 = 1.06 eV)**, suggesting that this pathway is kinetically more favorable. The initial activation step (IS1 → TS1) also follows a similar trend, with the formate pathway requiring

a higher barrier **(1.01 eV)** compared to the carboxyl pathway **(0.75 eV)**, further supporting the kinetic preference of the carboxyl route.

From a thermodynamic standpoint, notable differences are also observed between the two pathways. Although the formation of the first intermediate **(IS1 → FS1)** is exothermic in both cases, the formate pathway shows a larger stabilization **(−1.07 eV)** compared to the carboxyl pathway **(−0.39 eV).** However, the subsequent step **(FS1 → FS2)** is strongly endothermic in the formate pathway **(+1.64 eV)**, whereas it is only mildly endothermic in the carboxyl pathway **(+0.35 eV)**. As a result, the overall reaction energy **(IS1 → FS2)** is thermoneutral to slightly exothermic **(−0.04 eV)** for the carboxyl pathway, while it becomes endothermic **(+0.57 eV)** for the formate pathway. Activation barriers and reaction energies for both pathways are explicitly shown in **Figure 4.12.**

**Carboxyl Pathway**

| Step | Activation E (eV) |
|---|---|
| IS1→ TS1 | 0.75 |
| FS1→ TS2 | 1.06 RDS |

| Step | Reaction E (eV) |
|---|---|
| IS1→ FS1 | -0.39 |
| FS1→ FS2 | +0.35 |
| IS1→ FS2 | -0.04 |

Vs

**Formate Pathway**

| Step | Activation E (eV) |
|---|---|
| IS1→ TS1 | 1.01 |
| FS1→ TS2 | 1.83 RDS |

| Step | Reaction E (eV) |
|---|---|
| IS1→ FS1 | -1.07 |
| FS1→ FS2 | +1.64 |
| IS1→ FS2 | +0.57 |

Figure 4.12 Activation Energies and Reaction Energies of Formate and Carboxyl Pathway

Taken together, these results clearly demonstrate that the carboxyl pathway is both kinetically and thermodynamically more favorable than the formate pathway on the $Co@B_{12}N_{12}$ catalyst. The lower activation barriers and more favorable reaction energetics indicate that $CO_2$ reduction to formic acid preferentially proceeds via the carboxyl route, highlighting its

dominant role in the catalytic performance of the cobalt-doped nanocage. To provide a comprehensive comparison with the literature, the activation barriers of the suitable pathway of CO2 reduction reaction over different SACs are given in **Table 4.7.**

| M@Complex | Barrier for TS1 | Barrier for TS2 | 1st Reaction E | 2nd Reaction E | References |
|---|---|---|---|---|---|
| Co@$B_{12}N_{12}$ | 0.75eV | 1.06eV | -0.39eV | 0.35eV | This Work |
| Ti-NGF | 0.85eV | 0.08eV | +0.74eV | -1.16eV | [70] |
| Ni-G | 2.07eV | 0.017eV | 1.89eV | -1.96eV | [100] |
| Pt-G | 0.90eV | 0.14eV | 0.70eV | -0.91eV | [100] |

Table 4.7 Comparison of activation barriers and Reaction energies with literature

# 5 Conclusion

In this study, density functional theory (DFT) calculations were systematically employed to investigate transition-metal-doped $B_{12}N_{12}$ nanocages (Fe, Co, Ni, Cu, and Zn) as single-atom catalysts for $CO_2$ reduction to formic acid. Initially, interaction energy calculations were performed to evaluate the thermodynamic stability of the doped systems, which confirmed that Fe-, Co-, and Ni-doped nanocages form stable metal–cage complexes, whereas Cu and Zn exhibit weak physisorption and were therefore excluded from further catalytic investigation. Subsequent electronic structure analyses, including FMO and NBO charge analysis, revealed significant charge transfer from the metal centers to the nanocage, indicating enhanced reactivity and potential for molecular activation in the stable systems. Adsorption studies showed that among the active candidates, $Co@B_{12}N_{12}$ uniquely activates both $CO_2$ and $H_2$ molecules, as evidenced by pronounced C–O bond elongation in $CO_2$ and H–H bond elongation upon hydrogen adsorption. These findings were consistently supported by MEP, QTAIM, and IRI analyses, which confirmed the presence of partially covalent metal–adsorbate interactions and effective charge redistribution in the cobalt-doped system. Based on this consistent behavior across multiple analyses, $CO_2$ reduction was explored exclusively on $Co@B_{12}N_{12}$ through a Langmuir–Hinshelwood mechanism involving formate and carboxyl pathways. Comparative reaction energy profile analysis revealed that although both pathways are feasible, the carboxyl pathway is kinetically more favorable, exhibiting a lower rate-determining step (RDS) barrier of ~1.06 eV, compared to the formate pathway with an RDS barrier of ~1.83 eV. Overall, this work identifies $Co@B_{12}N_{12}$ as a promising, stable, and noble-metal-free single-atom catalyst for selective $CO_2$ reduction to formic acid. The detailed mechanistic insights provided by this study offer a valuable theoretical foundation for experimental researchers to design and develop efficient $B_{12}N_{12}$-based single-atom catalysts for sustainable $CO_2$ conversion.

# References


[1] V. Masson-Delmotte *et al.*, "Climate change 2021: the physical science basis," *Contrib. Work. Gr. I to sixth Assess. Rep. Intergov. panel Clim. Chang.*, vol. 2, no. 1, p. 2391, 2021.

[2] P. Friedlingstein *et al.*, "Global carbon budget 2024," *Earth Syst. Sci. Data Discuss.*, vol. 2024, pp. 1–133, 2024.

[3] J. Hansen, M. Sato, R. Ruedy, K. Lo, D. W. Lea, and M. Medina-Elizade, "Global temperature change," *Proc. Natl. Acad. Sci.*, vol. 103, no. 39, pp. 14288–14293, 2006.

[4] D. SC, "Ocean acidification: the other CO_2 problem," *Annu Rev Mar Sci*, vol. 1, pp. 169–192, 2008.

[5] C. Bellard, C. Bertelsmeier, P. Leadley, W. Thuiller, and F. Courchamp, "Impacts of climate change on the future of biodiversity," *Ecol. Lett.*, vol. 15, no. 4, pp. 365–377, 2012.

[6] M. Aresta, A. Dibenedetto, and A. Angelini, "Catalysis for the valorization of exhaust carbon: from CO2 to chemicals, materials, and fuels. Technological use of CO2," *Chem. Rev.*, vol. 114, no. 3, pp. 1709–1742, 2014.

[7] J. Qiao, Y. Liu, F. Hong, and J. Zhang, "A review of catalysts for the electroreduction of carbon dioxide to produce low-carbon fuels," *Chem. Soc. Rev.*, vol. 43, no. 2, pp. 631–675, 2014.

[8] E. V Kondratenko, G. Mul, J. Baltrusaitis, G. O. Larrazábal, and J. Pérez-Ramírez, "Status and perspectives of CO 2 conversion into fuels and chemicals by catalytic,

photocatalytic and electrocatalytic processes," *Energy Environ. Sci.*, vol. 6, no. 11, pp. 3112–3135, 2013.

[9] M. Grasemann and G. Laurenczy, "Formic acid as a hydrogen source–recent developments and future trends," *Energy Environ. Sci.*, vol. 5, no. 8, pp. 8171–8181, 2012.

[10] S. Zhang, P. Kang, and T. J. Meyer, "Nanostructured tin catalysts for selective electrochemical reduction of carbon dioxide to formate," *J. Am. Chem. Soc.*, vol. 136, no. 5, pp. 1734–1737, 2014.

[11] G. T. Rochelle, "Conventional amine scrubbing for CO2 capture," in *Absorption-based post-combustion capture of carbon dioxide*, Elsevier, 2016, pp. 35–67.

[12] F. Vega, M. Cano, S. Camino, L. M. G. Fernández, E. Portillo, and B. Navarrete, "Solvents for carbon dioxide capture," *Carbon dioxide Chem. capture oil Recover.*, vol. 32, pp. 137–144, 2018.

[13] B. Metz, O. Davidson, H. C. De Coninck, M. Loos, and L. Meyer, *IPCC special report on carbon dioxide capture and storage*. Cambridge: Cambridge University Press, 2005.

[14] M. Aresta, A. Dibenedetto, and A. Angelini, "The changing paradigm in CO2 utilization," *J. CO2 Util.*, vol. 3, pp. 65–73, 2013.

[15] S. Nitopi *et al.*, "Progress and perspectives of electrochemical CO2 reduction on copper in aqueous electrolyte," *Chem. Rev.*, vol. 119, no. 12, pp. 7610–7672, 2019.

[16] M. B. Ross *et al.*, "Designing materials for electrochemical carbon dioxide recycling,"

*Nat. Catal.*, vol. 2, no. 8, pp. 648–658, 2019.

[17] P. Saha, S. Amanullah, and A. Dey, "Selectivity in electrochemical CO2 reduction," *Acc. Chem. Res.*, vol. 55, no. 2, pp. 134–144, 2022.

[18] X.-F. Yang, A. Wang, B. Qiao, J. U. N. Li, J. Liu, and T. Zhang, "Single-atom catalysts: a new frontier in heterogeneous catalysis," *Acc. Chem. Res.*, vol. 46, no. 8, pp. 1740–1748, 2013.

[19] A. A. Peterson and J. K. Nørskov, "Activity descriptors for CO2 electroreduction to methane on transition-metal catalysts," *J. Phys. Chem. Lett.*, vol. 3, no. 2, pp. 251–258, 2012.

[20] Y. Hori, "Electrochemical CO2 reduction on metal electrodes," *Mod. Asp. Electrochem.*, pp. 89–189, 2008.

[21] W. Wang, S. Wang, X. Ma, and J. Gong, "Recent advances in catalytic hydrogenation of carbon dioxide," *Chem. Soc. Rev.*, vol. 40, no. 7, pp. 3703–3727, 2011.

[22] S. N. Habisreutinger, L. Schmidt-Mende, and J. K. Stolarczyk, "Photocatalytic reduction of CO2 on TiO2 and other semiconductors," *Angew. Chemie Int. Ed.*, vol. 52, no. 29, pp. 7372–7408, 2013.

[23] E. Roduner, "Understanding catalysis," *Chem. Soc. Rev.*, vol. 43, no. 24, pp. 8226–8239, 2014.

[24] S. M. J. Rogge *et al.*, "Metal–organic and covalent organic frameworks as single-site catalysts," *Chem. Soc. Rev.*, vol. 46, no. 11, pp. 3134–3184, 2017.

[25] H. Liu, X. Peng, and X. Liu, "Single-atom catalysts for the hydrogen evolution

reaction," *ChemElectroChem*, vol. 5, no. 20, pp. 2963–2974, 2018.

[26] W. Guo, Z. Wang, X. Wang, and Y. Wu, "General design concept for single-atom catalysts toward heterogeneous catalysis," *Adv. Mater.*, vol. 33, no. 34, p. 2004287, 2021.

[27] S. Ji, Y. Chen, X. Wang, Z. Zhang, D. Wang, and Y. Li, "Chemical synthesis of single atomic site catalysts," *Chem. Rev.*, vol. 120, no. 21, pp. 11900–11955, 2020.

[28] J. Li, J. J. Liu, and T. Zhang, "Preface to the special issue of the international symposium on single-atom catalysis (ISSAC-2016)," 催化学报, vol. 38, no. 9, p. 1431, 2017.

[29] B. Qiao *et al.*, "Single-atom catalysis of CO oxidation using Pt1/FeO x," *Nat. Chem.*, vol. 3, no. 8, pp. 634–641, 2011.

[30] J. Zhao and Z. Chen, "Single Mo atom supported on defective boron nitride monolayer as an efficient electrocatalyst for nitrogen fixation: a computational study," *J. Am. Chem. Soc.*, vol. 139, no. 36, pp. 12480–12487, 2017.

[31] Y. Li *et al.*, "High-valence nickel single-atom catalysts coordinated to oxygen sites for extraordinarily activating oxygen evolution reaction," *Adv. Sci.*, vol. 7, no. 5, p. 1903089, 2020.

[32] Y. Han *et al.*, "Hollow N-doped carbon spheres with isolated cobalt single atomic sites: superior electrocatalysts for oxygen reduction," *J. Am. Chem. Soc.*, vol. 139, no. 48, pp. 17269–17272, 2017.

[33] C. Zhao *et al.*, "Ionic exchange of metal–organic frameworks to access single nickel

sites for efficient electroreduction of CO2," *J. Am. Chem. Soc.*, vol. 139, no. 24, pp. 8078–8081, 2017.

[34] Z. Yu *et al.*, "Single-atom Ir and Ru anchored on graphitic carbon nitride for efficient and stable electrocatalytic/photocatalytic hydrogen evolution," *Appl. Catal. B Environ.*, vol. 310, p. 121318, 2022.

[35] F. Calle-Vallejo *et al.*, "Finding optimal surface sites on heterogeneous catalysts by counting nearest neighbors," *Science (80-. ).*, vol. 350, no. 6257, pp. 185–189, 2015.

[36] U. Heiz, A. Sanchez, S. Abbet, and W.-D. Schneider, "Catalytic oxidation of carbon monoxide on monodispersed platinum clusters: each atom counts," *J. Am. Chem. Soc.*, vol. 121, no. 13, pp. 3214–3217, 1999.

[37] M. Piernavieja-Hermida *et al.*, "Towards ALD thin film stabilized single-atom Pd 1 catalysts," *Nanoscale*, vol. 8, no. 33, pp. 15348–15356, 2016.

[38] X. Ma, Y. Lv, J. Xu, Y. Liu, R. Zhang, and Y. Zhu, "A strategy of enhancing the photoactivity of g-C3N4 via doping of nonmetal elements: a first-principles study," *J. Phys. Chem. C*, vol. 116, no. 44, pp. 23485–23493, 2012.

[39] H. Fei *et al.*, "Single atom electrocatalysts supported on graphene or graphene-like carbons," *Chem. Soc. Rev.*, vol. 48, no. 20, pp. 5207–5241, 2019.

[40] K. Pandiselvi, H. Fang, X. Huang, J. Wang, X. Xu, and T. Li, "Constructing a novel carbon nitride/polyaniline/ZnO ternary heterostructure with enhanced photocatalytic performance using exfoliated carbon nitride nanosheets as supports," *J. Hazard. Mater.*, vol. 314, pp. 67–77, 2016.

[41] X. Chen, S. Lin, and H. Zhang, “Screening of single-atom catalysts sandwiched by boron nitride sheet and graphene for oxygen reduction and oxygen evolution,” *Renew. Energy*, vol. 189, pp. 502–509, 2022.

[42] S. Saha and S. K. Pati, “Metal-doped fullerene: promising electrocatalysts for hydrogen and oxygen evolution reactions,” *Phys. Chem. Chem. Phys.*, vol. 27, no. 22, pp. 12024–12031, 2025.

[43] S. Sarfaraz, M. Yar, N. S. Sheikh, I. Bayach, and K. Ayub, “Transition metal-doped C20 fullerene-based single-atom catalysts with high catalytic activity for hydrogen dissociation reaction,” *ACS omega*, vol. 8, no. 15, pp. 14077–14088, 2023.

[44] P. Fallahi, H. Jouypazadeh, and H. Farrokhpour, “Theoretical studies on the potentials of some nanocages (Al12N12, Al12P12, B12N12, Be12O12, C12Si12, Mg12O12 and C24) on the detection and adsorption of Tabun molecule: DFT and TD-DFT study,” *J. Mol. Liq.*, vol. 260, pp. 138–148, 2018.

[45] H. T. Chiromo, “Metal organic frameworks (MOFs) supported single atom catalysts (SACs) for solar fuel conversion,” 2023, *Marquette University*.

[46] S. Sun *et al.*, “Single-atom catalysis using Pt/graphene achieved through atomic layer deposition,” *Sci. Rep.*, vol. 3, no. 1, p. 1775, 2013.

[47] J. Liu, “Catalysis by supported single metal atoms,” *Acs Catal.*, vol. 7, no. 1, pp. 34–59, 2017.

[48] J. Zheng *et al.*, “High loading of transition metal single atoms on chalcogenide catalysts,” *J. Am. Chem. Soc.*, vol. 143, no. 21, pp. 7979–7990, 2021.

[49] H. Zhang, G. Liu, L. Shi, and J. Ye, “Single-atom catalysts: emerging multifunctional materials in heterogeneous catalysis,” *Adv. Energy Mater.*, vol. 8, no. 1, p. 1701343, 2018.

[50] H. Yin *et al.*, “Ultrathin platinum nanowires grown on single-layered nickel hydroxide with high hydrogen evolution activity,” *Nat. Commun.*, vol. 6, no. 1, p. 6430, 2015.

[51] J. Liu, B. R. Bunes, L. Zang, and C. Wang, “Supported single-atom catalysts: synthesis, characterization, properties, and applications,” *Environ. Chem. Lett.*, vol. 16, no. 2, pp. 477–505, 2018.

[52] A. L. P. Silva, A. C. A. Silva, C. N. Navis, and J. de Jesus Gomes Varela Junior, “Theoretical study of putrescine and X12Y12 (X= Al, B and Y= N, P) nanocage interactions,” *J. Nanoparticle Res.*, vol. 23, no. 4, p. 108, 2021.

[53] A. L. P. Silva, N. de Sousa Sousa, and J. de Jesus Gomes Varela Júnior, “Theoretical studies with B12N12 as a toxic gas sensor: a review,” *J. Nanoparticle Res.*, vol. 25, no. 1, p. 22, 2023.

[54] W. Rakrai *et al.*, “Hydrogen storage and sensing ability of group 8B transition metal-doped B12N12 nanocages: a DFT investigation,” *Struct. Chem.*, vol. 35, no. 2, pp. 437–453, 2024.

[55] X. Liang *et al.*, “CO2 Adsorption on the B 1 2 N 1 2 Nanocage Encapsulated with Alkali Metals: A Density Functional Study,” *Nano*, vol. 14, no. 03, p. 1950034, 2019.

[56] M. Abbasi, E. Nemati-Kande, and M. D. Mohammadi, “Doping of the first row transition metals onto B12N12 nanocage: A DFT study,” *Comput. Theor. Chem.*, vol.

1132, pp. 1–11, 2018.

[57] N. De Sousa Sousa, A. L. P. Silva, A. C. A. Silva, and J. de Jesus Gomes Varela Júnior, “DFT analysis of dynamic, charge, and TD-DFT properties of doped, encapsulated, and decorated first-row transition metals on B12N12 nanocage: part 2,” *J. Inorg. Organomet. Polym. Mater.*, vol. 34, no. 8, pp. 3576–3588, 2024.

[58] S. Ali, R. Iqbal, A. Khan, S. U. Rehman, M. Haneef, and L. Yin, “Stability and catalytic performance of single-atom catalysts supported on doped and defective graphene for CO2 hydrogenation to formic acid: a first-principles study,” *ACS Appl. Nano Mater.*, vol. 4, no. 7, pp. 6893–6902, 2021.

[59] G. Chen, M. Buraschi, R. Al-Heidous, S. Bonakala, F. El-Mellouhi, and C. S. Cucinotta, “Efficient and Selective Electrochemical CO2 to Formic Acid Conversion: A First-Principles Study of Single-Atom and Dual-Atom Catalysts on Tin Disulfide Monolayers,” *J. Phys. Chem. C*, vol. 128, no. 38, pp. 15861–15872, 2024.

[60] D. N. Sredojević, Ž. Šljivančanin, E. N. Brothers, and M. R. Belić, “Formic acid synthesis by CO2 hydrogenation over single-atom catalysts based on Ru and Cu embedded in graphene,” *ChemistrySelect*, vol. 3, no. 9, pp. 2631–2637, 2018.

[61] M. D. Esrafili and B. Nejadebrahimi, “Theoretical insights into hydrogenation of CO2 to formic acid over a single Co atom incorporated nitrogen-doped graphene: A DFT study,” *Appl. Surf. Sci.*, vol. 475, pp. 363–371, 2019.

[62] W. Xun, X. Yang, Q.-S. Jiang, M.-J. Wang, Y.-Z. Wu, and P. Li, “Single-atom-anchored two-dimensional MoSi2N4 monolayers for efficient electroreduction of CO2 to formic acid and methane,” *ACS Appl. Energy Mater.*, vol. 6, no. 6, pp. 3236–3243,

2023.

[63] C. Zhao, X. Su, S. Wang, Y. Tian, L. Yan, and Z. Su, “Single-atom catalysts on supported silicomolybdic acid for CO 2 electroreduction: a DFT prediction,” *J. Mater. Chem. A*, vol. 10, no. 11, pp. 6178–6186, 2022.

[64] T. Liu, G. Wang, and X. Bao, “Electrochemical CO2 reduction reaction on 3d transition metal single-atom catalysts supported on graphdiyne: a DFT study,” *J. Phys. Chem. C*, vol. 125, no. 47, pp. 26013–26020, 2021.

[65] Z. Liu *et al.*, “Single-atom anchored on curved boron nitride fullerene surface as efficient electrocatalyst for carbon dioxide reduction,” *Mol. Catal.*, vol. 559, p. 114040, 2024.

[66] J. Zhang *et al.*, “High-dispersive Pd nanoparticles on hierarchical N-doped carbon nanocages to boost electrochemical CO2 reduction to formate at low potential,” *Small*, vol. 19, no. 37, p. 2301577, 2023.

[67] S. Zhou, X. Yang, W. Pei, J. Zhao, and A. Du, “Silicon nanocages for selective carbon dioxide conversion under visible light,” *J. Phys. Chem. C*, vol. 123, no. 15, pp. 9973–9980, 2019.

[68] X. Guo, H. Zhang, H. Yang, Z. Bo, J. Yan, and K. Cen, “Single Ni supported on Ti3C2O2 for uninterrupted CO2 catalytic hydrogenation to formic acid: A DFT study,” *Sep. Purif. Technol.*, vol. 279, p. 119722, 2021.

[69] K. Homlamai, T. Maihom, S. Choomwattana, M. Sawangphruk, and J. Limtrakul, “Single-atoms supported (Fe, Co, Ni, Cu) on graphitic carbon nitride for CO2

adsorption and hydrogenation to formic acid: First-principles insights," *Appl. Surf. Sci.*, vol. 499, p. 143928, 2020.

[70] M. D. Esrafili and L. Dinparast, "A DFT study on the catalytic hydrogenation of CO2 to formic acid over Ti-doped graphene nanoflake," *Chem. Phys. Lett.*, vol. 682, pp. 49–54, 2017.

[71] G. Yan, Z. Gao, M. Zhao, W. Yang, and X. Ding, "CO2 hydrogenation to formic acid over platinum cluster doped defective graphene: A DFT study," *Appl. Surf. Sci.*, vol. 517, p. 146200, 2020.

[72] J. Sirijaraensre and J. Limtrakul, "Hydrogenation of CO2 to formic acid over a Cu-embedded graphene: A DFT study," *Appl. Surf. Sci.*, vol. 364, pp. 241–248, 2016.

[73] A. Allangawi, K. Ayub, A. A. Al-Saadi, M. A. Gilani, and T. Mahmood, "CO2 reduction to CH4: Harnessing Fe1@ B12N12 as single atom catalyst for environment restoration," *Surfaces and Interfaces*, vol. 61, p. 106062, 2025.

[74] Y. Du and C. Chen, "CO2 Reduction Mechanism Based on a Partially Reduced Cu Single-Atom Catalyst: A First-Principles Study," *J. Phys. Chem. C*, vol. 129, no. 13, pp. 6211–6224, 2025.

[75] J. Shen, M. J. Kolb, A. J. Gottle, and M. T. M. Koper, "DFT study on the mechanism of the electrochemical reduction of CO2 catalyzed by cobalt porphyrins," *J. Phys. Chem. C*, vol. 120, no. 29, pp. 15714–15721, 2016.

[76] N. K. Singh, P. Kumar, A. Yadav, and V. C. Srivastava, "Multi-doped borophene catalysts with engineered defects for CO2 reduction: A DFT study," *J. Colloid*

*Interface Sci.*, vol. 654, pp. 895–905, 2024.

[77] C. Guo *et al.*, "Electrochemical CO2 reduction to C1 products on single nickel/cobalt/iron-doped graphitic carbon nitride: a DFT study," *ChemSusChem*, vol. 12, no. 23, pp. 5126–5132, 2019.

[78] L. Fu *et al.*, "Construction of Cr-embedded graphyne electrocatalyst for highly selective reduction of CO2 to CH4: A DFT study," *Chem. Eng. J.*, vol. 414, p. 128857, 2021.

[79] Y. Ren, X. Sun, K. Qi, and Z. Zhao, "Single atom supported on MoS2 as efficient electrocatalysts for the CO2 reduction reaction: A DFT study," *Appl. Surf. Sci.*, vol. 602, p. 154211, 2022.

[80] N. Kumari, N. Sinha, M. A. Haider, and S. Basu, "CO2 reduction to methanol on CeO2 (110) surface: a density functional theory study," *Electrochim. Acta*, vol. 177, pp. 21–29, 2015.

[81] M. J. Frisch *et al.*, "Gaussian 16, revision B. 01; Wallingford, CT, 2016," *There is no Corresp. Rec. this Ref.*.

[82] R. Dennington, T. Keith, J. Millam, and V. GaussView, "Semichem Inc," *Shawnee Mission KS, GaussView, Version*, vol. 5, no. 8, 2009.

[83] H. Tahir, N. Kosar, K. Ayub, and T. Mahmood, "Outstanding NLO response of thermodynamically stable single and multiple alkaline earth metals doped C20 fullerene," *J. Mol. Liq.*, vol. 305, p. 112875, 2020.

[84] H. Wu, X. Fan, and J.-L. Kuo, "Metal free hydrogenation reaction on carbon doped

boron nitride fullerene: A DFT study on the kinetic issue," *Int. J. Hydrogen Energy*, vol. 37, no. 19, pp. 14336–14342, 2012.

[85] A. S. Rad and K. Ayub, "Ni adsorption on Al12P12 nano-cage: a DFT study," *J. Alloys Compd.*, vol. 678, pp. 317–324, 2016.

[86] S. Grimme, "Semiempirical GGA-type density functional constructed with a long-range dispersion correction," *J. Comput. Chem.*, vol. 27, no. 15, pp. 1787–1799, 2006.

[87] A. A. Choir, S. R. Amelia, M. A. Martoprawiro, Y. Kusumawati, and A. L. Ivansyah, "Insight into the adsorption properties of CO2 and H2 gas on the B12Y12 (YN, P, As, Sb) nanocages from host-guest interaction perspective," *Int. J. Hydrogen Energy*, vol. 53, pp. 780–791, 2024.

[88] T. Lu and F. Chen, "Multiwfn: A multifunctional wavefunction analyzer," *J. Comput. Chem.*, vol. 33, no. 5, pp. 580–592, 2012.

[89] W. Humphrey, A. Dalke, and K. Schulten, "VMD: visual molecular dynamics," *J. Mol. Graph.*, vol. 14, no. 1, pp. 33–38, 1996.

[90] Y. Arshad, M. Asghar, M. Yar, T. Bibi, and K. Ayub, "Transition metal doped boron nitride nanocages as high performance nonlinear optical materials: a DFT study," *J. Inorg. Organomet. Polym. Mater.*, vol. 33, no. 4, pp. 943–955, 2023.

[91] N. De Sousa Sousa, A. L. P. Silva, A. C. A. Silva, and J. de Jesus Gomes Varela Júnior, "DFT analysis of structural, energetic and electronic properties of doped, encapsulated, and decorated first-Row transition metals on B12N12 nanocage: Part 1," *J. Inorg. Organomet. Polym. Mater.*, vol. 34, no. 9, pp. 4082–4099, 2024.

[92] M. Souri, “Investigation of nonlinear optical properties of a group of transition metal-decorated B12N12 nanocages: A DFT study,” *Phys. B Condens. Matter*, vol. 676, p. 415665, 2024.

[93] S. Uzun, Z. Esen, E. Koç, N. C. Usta, and M. Ceylan, “Experimental and density functional theory (MEP, FMO, NLO, Fukui functions) and antibacterial activity studies on 2-amino-4-(4-nitrophenyl)-5, 6-dihydrobenzo [h] quinoline-3-carbonitrile,” *J. Mol. Struct.*, vol. 1178, pp. 450–457, 2019.

[94] R. F. W. Bader, “Atoms in molecules,” *Acc. Chem. Res.*, vol. 18, no. 1, pp. 9–15, 1985.

[95] G. Henkelman, A. Arnaldsson, and H. Jónsson, “A fast and robust algorithm for Bader decomposition of charge density,” *Comput. Mater. Sci.*, vol. 36, no. 3, pp. 354–360, 2006.

[96] M. Ejaz *et al.*, “A rational design of metal doped C20 fullerene based sensor for the selective detection of ethyl butyrate as COVID-19 biomarker,” *Surfaces and Interfaces*, vol. 52, p. 104869, 2024.

[97] T. Lu and Q. Chen, “Interaction region indicator: a simple real space function clearly revealing both chemical bonds and weak interactions,” *Chemistry-methods*, vol. 1, no. 5, pp. 231–239, 2021.

[98] A. Sagaama, N. Issaoui, O. Al-Dossary, A. S. Kazachenko, and M. J. Wojcik, “Non covalent interactions and molecular docking studies on morphine compound,” *J. King Saud Univ.*, vol. 33, no. 8, p. 101606, 2021.

[99] M. Abedini, H. Tavakol, and D. Shirvani, “Theoretical study of Ni, Co and Cu single atom catalysts for CO2 to formic acid reduction,” *Surfaces and Interfaces*, p. 106726, 2025.

[100] M. D. Esrafili, F. Sharifi, and L. Dinparast, “Catalytic hydrogenation of CO2 over Pt- and Ni-doped graphene: a comparative DFT study,” *J. Mol. Graph. Model.*, vol. 77, pp. 143–152, 2017.

# Turnitin Originality Report

Document Viewer

Processed on: 09-Jan-2026 09:46 PKT
ID: 2854267968
Word Count: 13428
Submitted: 1

Exploring Metal Doped Nanocage as Single Atom... By Muqaddis Zahra Sp24-r06-012

| Similarity Index | Similarity by Source | |
|---|---|---|
| 13% | Internet Sources: | 2% |
| | Publications: | 12% |
| | Student Papers: | 1% |

include quoted | include bibliography | exclude small matches | mode:
quickview (classic) report | print | refresh | download

3% match (Ali Hussain, Muhammad Yar, Rayed S. Alshareef, Tariq Mahmood, Khurshid Ayub, R. Nawaz, Muhammad Yasin, Mazhar Amjad Gilani. "Efficient hydrogen splitting via single atom catalysts supported on Zn12O12 nanocage for sustainable clean fuel production", International Journal of Hydrogen Energy, 2024)
Ali Hussain, Muhammad Yar, Rayed S. Alshareef, Tariq Mahmood, Khurshid Ayub, R. Nawaz, Muhammad Yasin, Mazhar Amjad Gilani. "Efficient hydrogen splitting via single atom catalysts supported on Zn12O12 nanocage for sustainable clean fuel production", International Journal of Hydrogen Energy, 2024

1% match (Yue Zhang, Yirong Mo, Zexing Cao. " Rational Design of Main Group Metal-Embedded Nitrogen-Doped Carbon Materials as Frustrated Lewis Pair Catalysts for CO Hydrogenation to Formic Acid ", ACS Applied Materials & Interfaces, 2021)
Yue Zhang, Yirong Mo, Zexing Cao. " Rational Design of Main Group Metal-Embedded Nitrogen-Doped Carbon Materials as Frustrated Lewis Pair Catalysts for CO Hydrogenation to Formic Acid ", ACS Applied Materials & Interfaces, 2021

<1% match (Jijun Zhao, Qiuying Du, Si Zhou, Vijay Kumar. "Endohedrally Doped Cage Clusters", Chemical Reviews, 2020)
Jijun Zhao, Qiuying Du, Si Zhou, Vijay Kumar. "Endohedrally Doped Cage Clusters", Chemical Reviews, 2020

<1% match (Khalida Khalil, Béla Fiser, Magdalena Małecka. "Computational insights into solvent encapsulation and host–guest recognition by calix[4]arene", Scientific Reports, 2025)
Khalida Khalil, Béla Fiser, Magdalena Małecka. "Computational insights into solvent encapsulation and host–guest recognition by calix[4]arene", Scientific Reports, 2025

<1% match (Abdulrahman Allangawi, Khurshid Ayub, Abdulaziz A. Al-